RICE UNIVERSITY

Imaging and Manipulating Organometallic Molecules by Scanning Tunneling Microscopy

by

Corey J. Slavonic

A Thesis Submitted
in Partial Fulfillment of the
Requirements for the Degree

Master of Science

Approved, Thesis Committee:

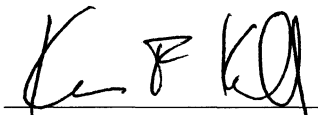

Kevin F. Kelly
Associate Professor of Electrical and
Computer Engineering

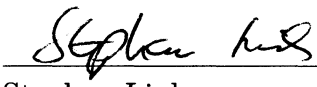

Stephan Link
Assistant Professor of Chemistry and
Electrical Engineering

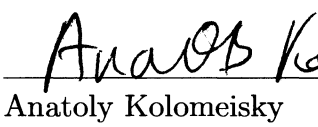

Anatoly Kolomeisky
Professor of Chemistry and Chemical and
Biomolecular Engineering

Houston, Texas

June, 2011

ABSTRACT

Imaging and Manipulating Organometallic Molecules by Scanning Tunneling Microscopy

by

Corey J. Slavonic

Using scanning tunneling microscopy (STM) we have explored complex surface adsorbed molecules, nanocars, on Au(111) and the parameters related to the direct translation of these molecules by the STM tip. Specifically, the molecules focused on here were functionalized with C_{60} or trans ruthenium complexes. With low tunneling currents the molecules could be imaged at room temperature. Increasing the tunneling current allowed us to bring the tip closer to individual molecules and reposition them on the surface. Below specific current and bias voltage conditions the molecules remained stationary, while in other cases the tip interaction was strong enough to drastically damage or eject the molecule from the field of view. High temperature scans revealed the effect of the wheel activation energy relative to the underlying surface as the different wheeled nanocars began diffusing at different temperatures confirming the manipulation measurements.

Contents

List of Figures

Chapter 1

Introduction

1.1 Motivation

Much of the work contained in this thesis involves investigating components that are much smaller than anything normally seen with a naked eye, or even with any sort of light microscope. The interests of these projects concern molecules which are no bigger than a few nanometers across. They live in a world where the wavelength of visible light is 100 times longer than the molecules themselves. While increasing the photon energy will decrease the wavelength, allowing one to resolve smaller objects, the energy required to bring the wavelength down <1 nm to resolve the molecules of interest would be about 1,240 eV, which is well into the X-Ray region and enough to ionize and destroy the molecules.

The solution is of course not to use light microscopes, but electron microscopes. Specifically, we employed the scanning tunneling microscope (STM) to image the molecules on a conducting surface. A STM is better suited than a scanning electron microscope[1] (SEM) or a transmission electron microscope[2] (TEM) for the type of studies we wanted to perform. An SEM cannot resolve the molecules of interest, while a TEM with its higher beam energy would probably destroy them. The basic technology of STM will be discussed in Section 2.2. An additional benefit of STM over other scanning probe techniques, such as atomic force microscopy (AFM), is its ability to perform simultaneous electrical measurements on samples.

---

[1] An SEM images the secondary or backscattered electrons with resolutions typically less-than tens of nanometers.

[2] A TEM images the electrons transmitted through the sample, providing sub nanometer resolution.

Throughout this work the STM was used to image individual molecules on a surface, manipulate them with the tip of the microscope, perform measurements, and explore a world at such a small length scale that the physics and chemistry of these systems is beyond our macroscopic intuition.

1.2 Introduction to STM

STM was the first of the various scanning probe techniques and employs an atomically sharp conducting tip to raster scan above a conducting surface with an applied voltage difference between the tip and the surface. The tip does not touch the surface, but stays around 10 Å away. The gap between the tip and sample presents a barrier to the electrons, which tunnel quantum mechanically from one to the other while a feedback system extends or lowers the tip to maintain the related current at a constant value, or simply measures the current as the surface changes. It is this tunneling phenomenon that allows the STM to obtain such amazing vertical and lateral resolution. The history and physics of the STM will be discussed in Sections 2.1 and 2.2. In addition to its imaging ability, being a local probe allows the STM to additionally interact and manipulate the atoms and molecules it images.

1.3 On the Manipulation of Complex Molecules

This thesis deals with several types of organic and organometallic systems designed to study molecular motion and rolling on surfaces. Given their structure, the molecules are commonly referred to as nanocars, of which there are several types. The newest variation discussed in this report has a ruthenium based wheel unit surrounded by nine phenyl groups resulting in a paddle-wheel like structure (Figure 4.1). We compare this ruthenium wheeled nanocar (RuNC) to the well-studied type of C_{60} wheeled nanocar (C60NC) (see Figure 4.2). The gap resistance (see Section 2.3.1), which reflects the proximity of the tip to the molecule, required to laterally translate the two molecules is explored and compared. An additional ensemble comparison of the two molecules is

obtained by imaging their surface motion response at elevated temperatures. Lastly, the relative chemical stability of the two molecules is discussed, as well as the potential future applications of this work.

1.4 Overview

Here is a brief guide to the contents of this thesis. Chapter 2 will deal with the basic history and technology of the STM, and provide an overview of the sort of systems it was designed to explore, as well as some contributions to science it has provided. Here we will also explore some advanced STM techniques used during the course of this work, as well as complimentary nanoscale techniques and measurements that provide insight into the STM results. Chapter 3 will provide a background on the nanocar family of molecules, including previous STM work, fluorescence studies, and related compounds. Chapter 4 will exhibit the bulk of the experiment work performed including the imaging of a new type of nanocar under various conditions. We will show how the organometallic nanocar compares to previous versions, as well as the parameters required to laterally translate the molecule on a surface. The potential problems dealing with surface interactions and aggregate control will also be discussed. Lastly, Chapter 5 will give a summary of our results and provide future directions for the projects.

Chapter 2

Background

2.1 A Brief History of the Scanning Tunneling Microscope

2.1.1 Inception

The STM technique requires quantum mechanics, and in fact is not even describable using classical or relativistic physics. Quantum tunneling describes the phenomenon where particles can "tunnel" through barriers without ever actually "residing within" them. According to [1],

> The idea that quantum mechanics should permit particles to pass through barriers occurred to J. R. Oppenheimer during a drive from the eastern United States to a position as research fellow at Cal. Tech. in 1927. The symbols
>
> $$i \sim \exp\frac{-C}{E}$$
>
> See Davis (1968), p. 23. The tunneling formula in more familiar notation might be read $\psi \sim \exp[-x\sqrt{2mU/\hbar^2}]$
>
> had just been scrawled on the windshield of his car when he ran off the road into a county courthouse, a rather unsuccessful first attempt to put the formula into practice.

Heinrich Rohrer, while working for the IBM Zurich Research Laboratory in Rüschlikon, Switzerland in the late 1970s, became interested in the quantum tunneling phenomenon, and its applicability to studying surface oxides, josephson junctions, and thin films on surfaces. Quantum tunneling had become a topic of interest for

many in the superconductor and vacuum community [2, 3] and so Rohrer, in 1978, hired Gerd Binnig, himself holding similar interests, with the hopes of developing a device to perform local measurements on many of these interesting systems. Though the original goal [4] of Binnig and Rohrer was to build a device capable of performing local electronic spectroscopy on superconductors, thin films, and oxides, they quickly realized that they could incorporate topographic scanning with unparalleled lateral and vertical resolution through the use of piezoelectric elements [5–7]. In 1972 Russel Young had taken many similar steps and developed the "Topografiner," a device reminiscent of what Binnig and Rohrer's STM would become but missing some key elements; the Topografiner used high voltages and so operated in the field-emission regime, thus lacking the resolution needed to make the kind of local measurements Binnig and Rohrer desired. Had Young's funding not been cut it is likely that his team would have built a device similar in capability to the modern STM. In 1982 Binnig and Rohrer published their work on the STM [8], but the response from the scientific community, and surface scientists in particular, was lackluster. Many were skeptical of the device, but Binnig and Rohrer actively used their invention to investigate surfaces and oxides, as was their dream, and knew that the discoveries it could bring would lead to its acceptance.

2.1.2 The Si(111) 7×7 Problem

One outstanding problem in surface science at the time was properly identifying various surface reconstructions. When a solid is cleaved, the exposed, previously bulk, atoms are typically no longer in energetically favorable positions and so will physically shift positions to minimize their energy. Prior to the STM, scientists had measured the structure of cleaved surfaces using low energy electron diffraction [9] (LEED), which related the positions of the atoms to diffraction peaks in Fourier space. The problem was that only the magnitude of the Fourier space representation was quantifiable, meaning that the phase information in Fourier space was lost and so

too was the relative shift of the atoms in real space. The result being that multiple reconstructions could result in the same LEED image. One surface that was under heavy investigation was the Si(111) surface. It was known that one of the more stable reconstructions was a 7×7, so 49 atoms made up a unit cell, and thus a staggering number of possible reconstructions could give the Si(111) 7×7 LEED pattern. The problem exhausted the techniques of the day [10–14], and a great many theoretical models were offered to explain the results [15–18]. In 1983 Binnig and Rohrer added their contribution [19], the first real-space images of the reconstructed silicon surface, taken by STM. Their data revealed each unit cell possessed 12 atoms, which none of the models had predicted, and offered an unprecedented insight into the physics of surface reconstruction. The final details of the structure were worked out by Takayanagi, et al. [20], and has become the dimer-adatom-stacking fault (DAS) model (see Figure 2.1).

Binnig and Rohrer went on to receive the 1986 Noble Prize[1] in Physics *"for their design of the scanning tunneling microscope"* [4, 21].

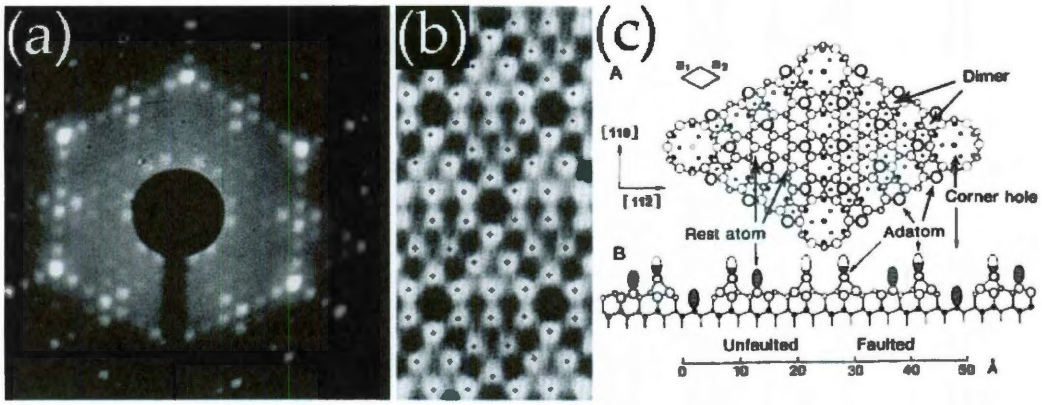

Figure 2.1: (a) The LEED pattern for the Si 7x7 surface [22]. (b) Binnig and Rohrer's STM image of the Si 7x7 surface [19]. (c) Takayanagi's DAS model, showing the 9 dimers, 12 adatoms, and the faulted and unfaulted halves (modified from [20] & [23]).

[1]Each received $^1/_4$ the prize, with the other half going to Ernst Ruska *"for his fundamental work in electron optics, and for the design of the first electron microscope"* [21].

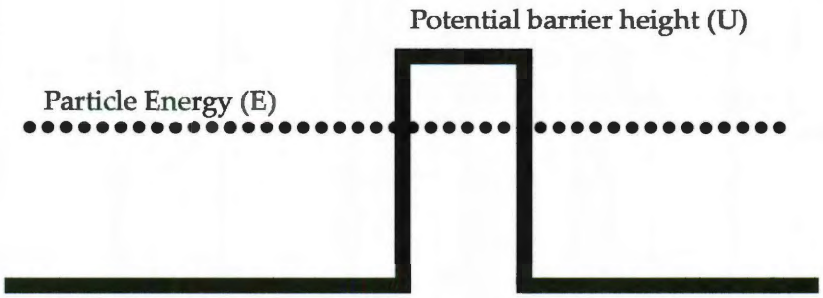

Figure 2.2: A one dimensional finite potential barrier.

2.2 The Basic Physics of STM

2.2.1 Quantum Tunneling

In quantum mechanics electrons can be described by wave functions which must satisfy the Schrödinger equation, which in one dimension is

$$-\frac{\hbar^2}{2m}\frac{d^2}{dx^2}\psi(x) + U(x)\psi(x) = E\psi(x). \tag{2.1}$$

If the electron were free then equation 2.1 will have plane wave solutions of the form

$$\psi(x) = \psi_0 e^{\pm ikx} \tag{2.2}$$

where the wave number is

$$k = \frac{\sqrt{2m(E-U)}}{\hbar}. \tag{2.3}$$

If the electron were to encounter a potential barrier, as in Figure 2.2 , then there would be a separate, *non-zero* solution for $\psi(x)$ in the barrier region

$$\psi_b(x) = \psi_0 e^{-\kappa x} \tag{2.4}$$

$$|\psi_b(x)|^2 = |\psi_0|^2 e^{-2\kappa x} \tag{2.5}$$

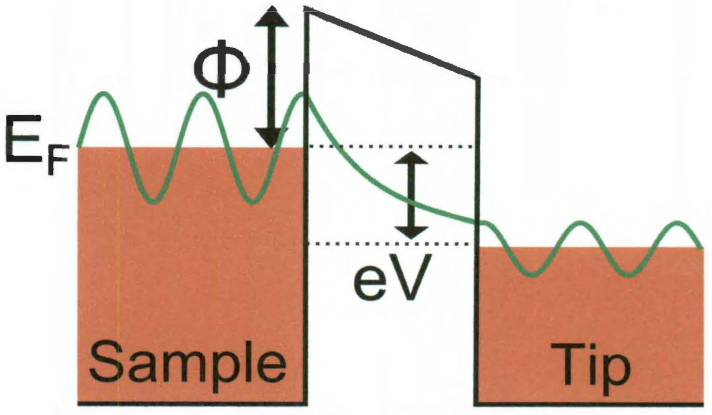

Figure 2.3: Metal-vacuum-metal tunneling from a sample to a tip. The wave function decays upon entering the barrier, but continues at smaller amplitude in the tip. The Fermi energy, E_F, is the energy of the highest filled state at $T = 0$, and the work function, ϕ, is the energy required to remove an electron from the metal to the vacuum level. V is the applied voltage difference between the tip and the sample, while eV is the energy difference.

where

$$\kappa = \frac{\sqrt{2m(U-E)}}{\hbar}. \tag{2.6}$$

As the absolute value squared of $\psi_b(x)$ is non-zero in the barrier region there exists a possibility that the electron could be found inside the barrier, though unlike equation 2.2, $|\psi_b(x)|^2$ decreases to zero as the electron moves through the barrier. If the barrier is thin enough the electron will have some probability at the far side and will be able to continue on its trajectory, albeit with a lower energy. This is quantum tunneling. In classical physics the electron would simply have been reflected at the barrier, but here there is a small chance the electron will pass through the high potential barrier.

Taking the metal-vacuum-metal tunneling junction, as seen in Figure 2.3, as an example STM system the barrier height $U - E$ is approximately the work function ϕ when $eV \ll E_F$. Replacing this in equation 2.6 gives

$$\kappa = \frac{\sqrt{2m\phi}}{\hbar} \tag{2.7}$$

which has a value of about 11.4 nm^{-1} after applying a typical metal work function of about 5 eV [23]. Plugging that into equation 2.5 shows that $|\psi_b(x)|^2$ decays about an order of magnitude for every Å of separation. Thus the tunneling current measured between the tip and sample is extremely sensitive to the tip height above the surface and this is part of what gives STM its spectacular vertical resolution.

2.2.2 Image Formation

When a bias is applied between the tip and the sample a tunneling current will flow. In the simplest configuration this current is read as the tip sweeps over the surface, giving a map of tunneling current vs. location. This type of scanning is called constant height imaging, as the tip height does not change. This presents problems with samples that are not *perfectly* atomically flat, which if you are interested in adatoms, molecular electronics, oxides, etc, is most samples. The second type of scanning involves a feedback circuit to move the tip away from (towards) the surface when the current increases (decreases). This is called constant current imaging, and is the most popular mode of operating an STM. The actual mechanism for moving the tip such small distances is accomplished with a piezoelectric scanner (see [23] for various designs).

The actual image in the constant current mode is a map of the displacement of the tip versus position over the surface. If the tip were swept across a protrusion on the surface, decreasing the tip/sample distance, the current would increase and the tip would be withdrawn. Likewise, while sweeping across a depression the current would decrease and the tip would be extended. This STM image should not immediately be associated only with the topography of the surface though, as a spot with a higher (lower) conductivity would also cause the current to increase (decrease) and the tip to be withdrawn (extended). In 1961 Bardeen [24] determined the tunneling current across a barrier by splitting the Schrödinger problem into two systems. Using time-dependent perturbation theory he could calculate the tunneling current by finding the

tunneling matrix element from the overlap of the tip/surface wave functions. Using Fermi's golden rule and summing over all states he found the tunneling current,

$$I = \frac{4\pi e}{\hbar} \int_{-\infty}^{\infty} [f(E_F - eV + \epsilon) - f(E_F + \epsilon)] \times \rho_S(E_F - eV + \epsilon)\rho_T(E_F + \epsilon)|M|^2 d\epsilon \quad (2.8)$$

where f is the Fermi function[2] and ρ is the density of states[3] of the sample and tip respectively. Even at room temperature k_BT is much smaller than typical scanning voltages[4] so the Fermi functions can be approximated with step functions. Bardeen also assumed that the tunneling matrix element $|M|$ does not change dramatically within the region $\pm eV$ of E_F, so equation 2.8 can be rewritten as

$$I \propto \int_0^{eV} \rho_S(E_F - eV + \epsilon)\rho_T(E_F + \epsilon) d\epsilon. \quad (2.9)$$

The elegance of this equation is the symmetry between ρ_S and ρ_T. Both the tip density of states and the sample density of states are equally important to the value of the tunneling current. This also brings to light some of the utility of using STM as a tool to probe the local density of states through the tunneling current, a technique known as scanning tunneling spectroscopy (STS). For more details on the physics of STM see [23, 25]

2.2.3 Nanoscale Forces

Another aspect of STM lies in its nature as a local probe and the associated intermolecular forces present at the atomic scale. The van der Waals force, the Pauli repulsion force, and the possibility of covalent bonding between the tip and surface must all be taken into account when analyzing STM images.

The van der Waals force arises from charge fluctuations in the atomic electron

---

[2] $f(E) = (1 + e^{(E-E_F)/k_BT})^{-1}$

[3] The number of electrons per unit volume per unit energy

[4] 300 K $\times$ k_B = 0.025 eV $\ll$ 1 eV

cloud [26]. These fluctuations induce dipoles in nearby atoms which are then attracted to the original. Between two particles the van der Waals energy U is proportional to $-r^{-6}$, but between a circular tip and a surface the energy is $U = -\frac{HR_c}{6R}$ where R_c is the radius of curvature of the tip and the Hamaker constant H is $\approx$ 2-3 eV [23]. At typical STM tip/sample distances the van der Waals energy is of the order of 0.01-0.02 eV.

The Pauli repulsion force arises from the Pauli exclusion principle between the electron clouds of nearby atoms. It is generally approximated by the r^{-12} term in the Lennard-Jones potential[5].

The covalent, or chemical, bond can be described as a resonance from an electron tunneling between two atoms. The resonance gives rise to a bonding and anti-bonding states, of which the bonding state is a lower energy and stabilizes the molecule [27].

2.3 A Feynman Machine and 35 Atoms

2.3.1 Lateral Manipulation

One can begin with a clean metal surface and deposit atoms on it randomly. These adatoms (adsorbed atoms) sit on specific adsorption sites of minimum potential energy. Typically these sites are either on-top, bridge, or hollow sites (see Figure 2.4) and possess the various symmetries associated with the underlying surface lattice. The height of the potential well, or the energy that must be applied to move the adatom laterally out of the well, is known as the diffusion barrier. The energy required to remove the adatom from the surface is known as the heat of adsorption, or adsorption energy. We are interested in height of the diffusion barrier[6], as it must be overcome to move the adatom to an adjacent site. The diffusion barrier for single adatoms on a surface range from ~10 meV to 1 eV [28]. Typically the adatoms will

[5] $U(r) = -\frac{a}{r^6} + \frac{b}{r^{12}}$

[6] Also known as the corrugation barrier or diffusion activation energy [28].

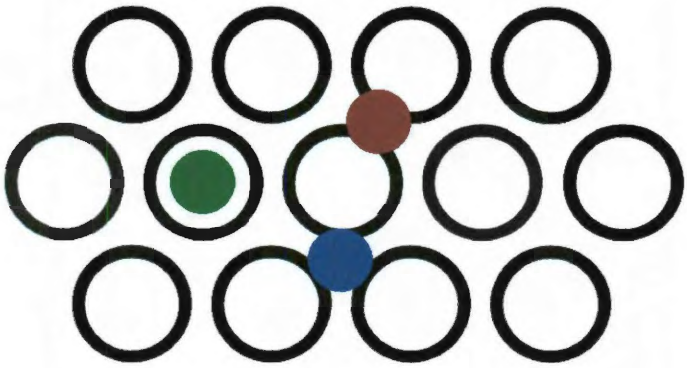

Figure 2.4: A image of the possible adsorption sites on a close packed surface, the black circles are top layer atoms. The green dot is an on-top site, directly above the surface atom, the red dot is a bridge site, between two adjacent surface atoms, and the blue dots is a hollow site, between 3 adjacent atoms.

also have some thermal energy as well and if that energy is less than the diffusion barrier they will be stable at their adsorption site. If the adatom has a higher thermal energy than the diffusion barrier then it slides around the surface, not stopping for long at any particular site. Even an adatom with less thermal energy than the diffusion barrier has some probability of hopping to an adjacent site, the process of surface diffusion.

The STM tip is $\sim$1 nm from the surface and atomically sharp so it can move adatoms to different adsorption sites by providing the energy to overcome the diffusion barrier in a controlled way [29]. The first step is to locate a suitable adatom through regular scanning. Once found, the tip is manually brought over the adatom and the z piezotube is extended to decrease the adatom/tip distance. The force between the tip and adatom increases as the distance between them decreases. When the tip/adatom interaction energy is equal to the diffusion barrier the tip is laterally translated over the surface. Upon reaching the destination the z piezotube is retracted, decreasing the tip/adatom interaction energy and allowing the surface adsorption site to take over (see Figure 2.5). In this simplistic view the only variables we have for controlling

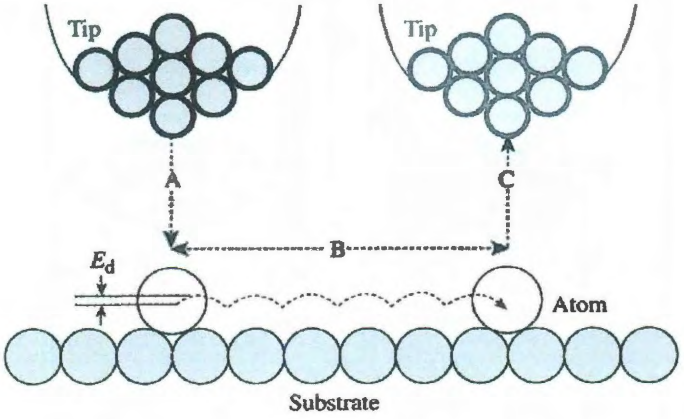

Figure 2.5: In motion A the tip is brought close to the adatom by increasing the tunneling current until the interaction energy is equal to E_d (diffusion barrier), then (B) translated across the surface, and finally (C) withdrawn to leave the adatom in the new location. Image from [23].

the vertical height of the tip are the bias voltage and the tunneling current[7]; nothing is known about the interaction energy or absolute tip/sample distance. There is one parameter though that can be used to compare different tip manipulation events: the gap resistance

$$R_{gap} = \frac{V_{bias}}{I_{tunneling}}. \tag{2.10}$$

In fact any set of bias and current that leaves the gap resistance unchanged will be able to apply the same interaction energy to move the adatom within the limit of certain assumptions. This is known as the threshold resistance [28, 30] and is the primary means of determining interaction strength in STM [31, 32]. Typical threshold resistances for a single atom on a metal surface at cryogenic temperatures range from 19 kΩ to 5000 kΩ [23]. By looking at the gap resistance required to move different types of molecules we can gauge their relative surface interaction strength.

[7]The tip height is controlled through the feedback circuit and is a function of the tunneling current.

By recording the manipulation parameters over many attempts we can develop a picture that reflects the molecular reaction to the tip and the type of motion that occurs. There are several more nuances, such as the following: if there is a threshold voltage, above which the molecules move mostly independent of the current, then the tip is pushing/pulling due to the electric field around the tip [33]; if there is a threshold current, above which the molecules move mostly independent of the bias voltage, then the molecules are responding to electron injection; if there is a threshold gap resistance, above which the molecules don't respond, then the mechanism is a van der Waals interaction [31, 34] and simply depends on tip distance.

2.3.2 The Smallest Logo Ever

The first people to use the STM tip to exert intentional control over a surface were Becker, et al. [35], at AT&T Bell Laboratories, who increased the bias voltage above 4 V on a Ge(111) surface to create a raised protrusion. The protrusion was a pile of germanium atoms previously transferred to the tip that were repelled due to the high voltages. This method of increasing the bias voltage to remove contaminates from the tip has become a staple method of cleaning STM tips *in situ*. A year later a research team at the IBM Almaden Research Center [36] demonstrated that it was possible to pin organic molecules to a graphite surface by applying a +3.5 V pulse. The molecules, either attached to the tip or free on the surface, could not be seen until a 3.5 V pulse was applied, after which one would appear at the site of the pulse and remain until a second pulse of similar voltage was applied.

Two years later, controlled lateral manipulation of a single atom was performed by Eigler and Schweizer [37], while at IBM Almaden, on xenon atoms adsorbed on Ni(110) at 4 K. Using 35 xenon atoms Eigler spelled out the letters IBM on the nickel surface, each letter being only 5 nm tall. Many complex patterns were soon created out of individual atoms on surfaces [38], and even larger, more complicated molecules have since been manipulated [39, 40].

2.4 The Kelly Lab

2.4.1 Instruments

The majority of the experiments conducted for this thesis were performed under ultra-high vacuum[8] (UHV) on a UHV-300 model RHK[9] STM of the Besocke style[10] [42]. There are four piezo tubes, three outer tubes at the points of an equilateral triangle and a center tube for scanning (see Figure 2.6). The outer tubes are used for the course motion of bringing the tip into range of the sample[11]. They work by a stick-slip mechanism where the legs smoothly bend one direction with the ball bearings stationary, then the legs suddenly switch directions. The ball bearings now slide across the sample holder's ramps while the legs have positioned themselves behind. They slowly move forward, and then whip the ball bearings in front of them again (see Figure 2.6(c)). By repeating this process the head can lower or raise itself. This design also provides mechanical stability and good vibration isolation. The voltage waveforms supplied by the RHK control unit can be customized to change the "step" length of the legs, as well as to walk in the cardinal directions to reposition the tip on the surface.

Our chamber is additionally equipped with an ion gun possessing a feed line connected to an argon gas cylinder. The ion gun was used to bombard noble metals surfaces with ionized Ar atoms accelerated through a 1-5 kV potential. This would sputter the surface metal atoms allowing us to remove contamination layers from the sample.

---

[8] $<10^{-9}$ torr, see [41] for an introduction to UHV systems and pumps.

[9] `www.rhk-tech.com`

[10] Also known as a beetle style, or walker style.

[11] The piezotubes used have a z-range of <1 μm.

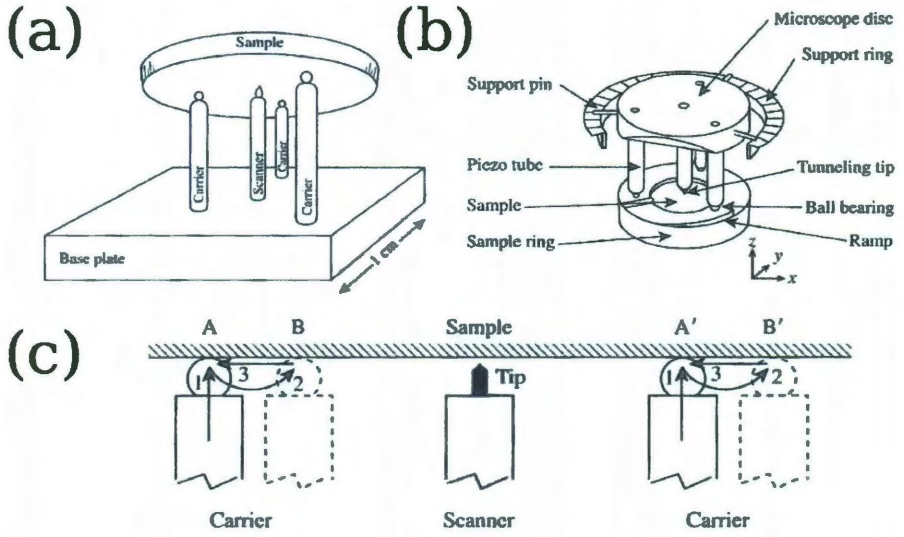

Figure 2.6: In (a) is shown a simple schematic of the Besocke style scanning head, with the 3 outer legs and the one inner scanning tube. (b) shows the setup used in the RHK UHV-300 system. Specifically the head is lowered onto the ramped sample holder with a linear translator in vacuum, the legs land at the tops of the sample holder's ramps. Using stick-slip motion (c) the head lowers itself to bring the tip closer to the sample. Figures from [23, 42].

2.4.2 Au(111)

The principle substrate used throughout this work was the Au(111) surface because of its inert nature and ease of preparation. The interaction energy with a specific class of molecular fullerenes, C_{60}, at room temperature is ideal for diffusion and motion experiments as individual C_{60} molecules latch into clusters and diffuse rapidly, only becoming stationary when the cluster size reaches > 8 molecules [43].

The Au(110) surface was one of the first explored by STM [8] but atomic resolution on the close packed FCC (111) facet would not be achieved until 1987 [45] due to its weaker atomic corrugation. Like the Si(111) 7×7 surface, the Au(111) surface had proven difficult to decipher as it exhibited a $22\times\sqrt{3}$ [46] reconstruction. It was the only known (111) metal surface to undergo a reconstruction, and in 1987 it was only

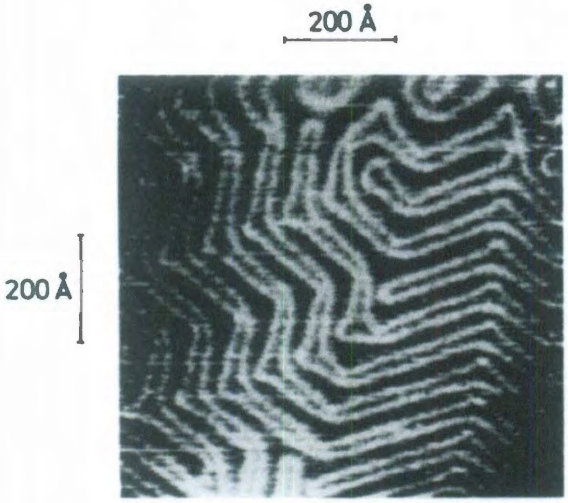

Figure 2.7: The Au(111) herringbone reconstruction by [44]. The bright lines are the transition between FCC (wider) and HCP (thinner) regions and have a transverse period of 6 nm. They are rotationally separated by 120°.

the second close packed (111) surface to be imaged with atomic resolution. Through LEED studies it was known that the reconstruction was anisotropic and resulted in an oscillation of the packing density of the surface atoms, which was confirmed by Wöll, et. al. [47], though they could not resolve the atomic positions inside the oscillations. The final piece of the puzzle was put in place by Barth, et. al. [44], who determined the atomic positions were oscillating due to a surface transition from FCC to HCP every 6 nm. These oscillations occurred over the clean Au(111) surface with an apparent corrugation of 0.2 Å. Even more interesting was that the corrugation formed a superstructure over the surface with different rotation domains separated by 120° as in Figure 2.7. This is know as the herringbone reconstruction.

2.4.3 Sample Preparation and Creation

Most of the work in this thesis involved scanning molecules deposited onto Au(111), but before they could be deposited the Au had to be clean. Seeing as we were trying to resolve single molecules only a few nanometers in size, any contamination on the surface could potentially interfere with imaging and manipulation. This required us to have atomically clean Au, the metric being the resolution of the herringbone

reconstruction.

The atomically flat Au(111) is created by depositing Au onto mica at >400 °C. We purchased Au(111) through Agilent[12]. In air, the Au was hydrogen flame annealed [46] for ~10 mins and then loaded into the STM. Additional cleaning steps for UHV STM involved Ar^+ sputtering and annealing where the Au surface was heated to ~400 °C, sputtered with 1.5 kV Ar^+ ions and then annealed at >400 °C[13]. The sputtering and annealing was repeated for several 5-10 min cycles. If the sample was first being introduced into UHV then a 1-4 hr out-gassing of the sample and holder was carried out at ~100 °C beforehand.

Molecular deposition involved one of the following four procedures: drop casting, spin casting, dunking, or vacuum depositing. Drop casting is the simplest where the molecules are mixed into a solvent and directly dropped onto the surface from a pipette. For spin casting, the sample was secured to a spinning plate and then the molecules were deposited onto the spinning sample which enabled a more uniform distribution of molecules. Preparation by dunking involved placing the sample into a v-vial of solvent. This method was mostly reserved for depositing alkanethiol SAMs onto Au.

The primary method of depositing the nanocar molecule was through vacuum dosing wherein a small amount of solvent (1-2 ml) was placed into a chamber sealed with a poppet valve at one end (see Figure 2.8). A burst of current through a coil of wire around the chamber created a magnetic field which pulled the poppet valve back to allow the solvent to flow out. The valve was placed ~10 cm from the sample surface which was under a vacuum of $\sim 3 \times 10^{-7}$ torr. The methods for controlling the surface concentration were adjusting the concentration of molecules in the solvent, adjusting the amount of time the poppet was open, and opening the poppet more

[12]Agilent Technologies Gold-coated substrates with 1500 angstroms of Au (111) Covering 2.0 cm x 2.1 cm; cut to ~0.5 cm × 0.5 cm to fit sample holders.

[13]Typically not much hotter than 500-600 °C as above that temperature the Au would be blown off the mica backing.

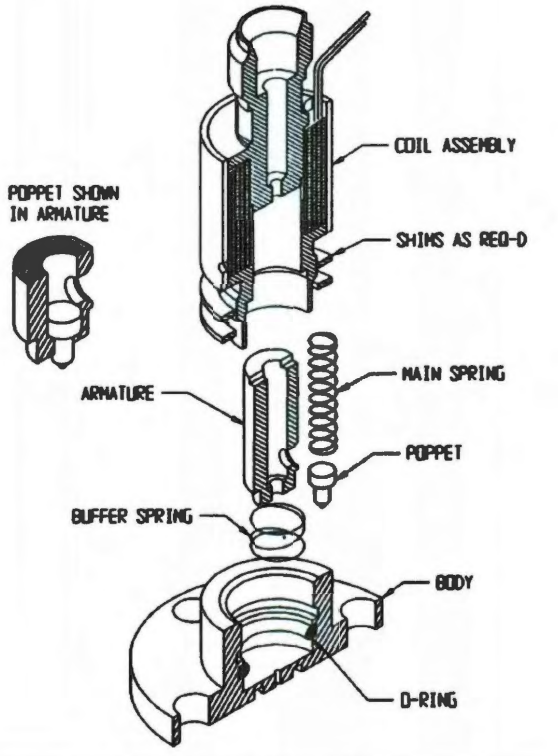

Figure 2.8: A dosing valve schematic showing the poppet and coil assembly.

than once. Typical parameters for nanocar deposition were 2 bursts of 15-25 ms at 3 V. See [48–50] for additional details of usage. We used a solenoid pulse valve purchased from Parker[14] attached to the load lock of the UHV chamber.

2.4.4 Tip Preparation

The tips were mechanically sharpened 80% by weight Pt/20% Rd or Ir spindles 0.25 mm in diameter, purchased from Alfa Aesar. They were cleaved with wire cutters in air to a length of ~0.5 cm and placed into the tip holder.

[14] www.parker.com

Chapter 3

The Nanocar Family History

An understanding of the surface effects on single molecules is important for designing self-assembled systems and is exemplified by systems such as alkanethoils on Au, graphene growth on silicon carbide through silicon evaporation, carbon nanotube growth, and all biological systems. Achieving self-assembly of nanoscale systems is perhaps the only way to realize applications out of the lab. It was for the understanding of molecular surface interactions related to rolling and sliding, for the usage of and control of molecular machines, that the Tour group at Rice University first synthesized the nanocar.

3.1 Background

Work on the first nanocar began in the hopes of producing, understanding, and controlling molecular systems capable of directed movement on the nanoscale of which the simplest examples include translating a target molecule on the surface without STM tip interference and creating or breaking molecular bonds through interaction with the molecular components. The properties of the surface diffusion of molecules were well known, but to actually control the surface molecules represented an appreciable challenge. STM tip manipulation of individual molecules represented a real advance in the field, but single molecules were a far cry from true ensemble dynamics by synthetic molecular machines.

Initial studies started with a readily available nanoscale wheel-like molecule, buckminsterfullerene[1]. Several fullerene-wheeled variations were produced (Figure 3.1)

[1] a.k.a. bucky balls, a.k.a. C_{60}

which interacted in different ways with the surface and even possessed the potential to transport other atoms or molecules with them. All of these molecules proved interesting in their own way, but much of the work was focused on the four-wheeled nanocar, which we will review here. For a review of the other C_{60}-based molecules shown please see [51,52]. The initial studies of the nanocar involved basic characterization, tip manipulation, scanning at elevated temperatures, along with investigations of apparent C_{60} height and OPE chassis flexibility.

3.2 Surface Rolling Molecules

The first work on the nanocar was published in 2005 [50] and explored the nanocar and trimer at room and elevated temperatures. The molecules were stationary at room temperatures with scanning conditions of 0.4 V and 10 pA, but after annealing to above 170 °C the nanocar became mobile, both laterally translating and pivoting on the surface. Interestingly, the trimer **A** molecules almost exclusively rotated in place above 225 °C while the trimer **B** molecules showed no motion up to 300 °C at which point they began to decompose. Tip manipulation parallel to and perpendicular to the axles was performed on a nanocar with a gap resistance of 28.5 MΩ. The attempts parallel to the axle resulted in no motion while the attempts perpendicular to the axles resulted in the molecule moving with the tip as expected. This was strong evidence for an anisotropic barrier to diffusion, higher parallel to the axles and lower perpendicular to, which coincided well with the idea that the C_{60} wheel units were spinning freely and thus facilitating rolling motion across the surface.

3.3 The Next Generation

To explore the idea further the Tour group began synthesizing another type of nanocar with *p*-carborane chosen as the wheel unit. Though the cage-like carborane is not a fullerene, it was thought that the molecule could behave similar to C_{60} and undergo rotational motion. Physically, the molecule is slightly smaller than buckminster-

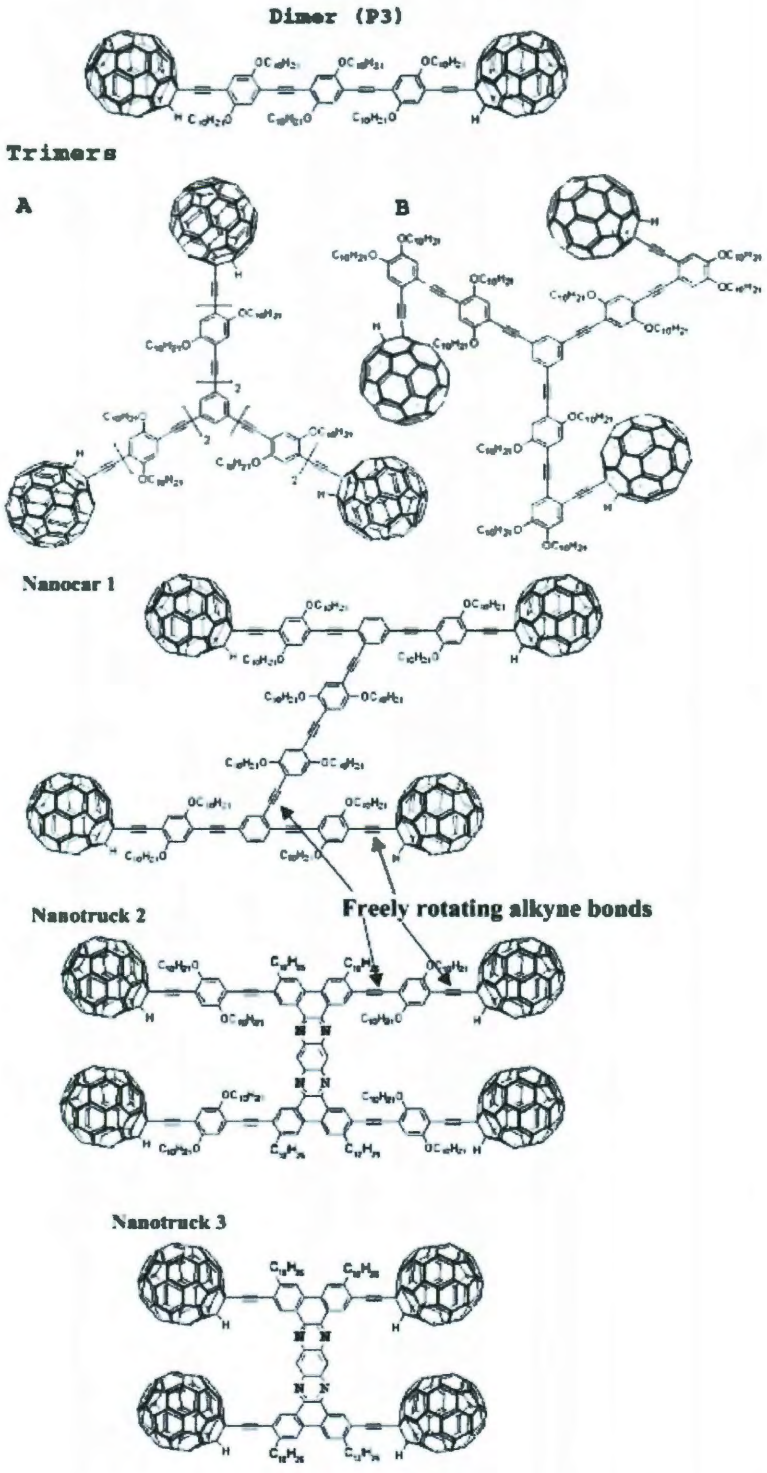

Figure 3.1: Several variations of C_{60} based molecules including: dimers, trimers, nanocars, and nanotrucks. Figures from [51, 52].

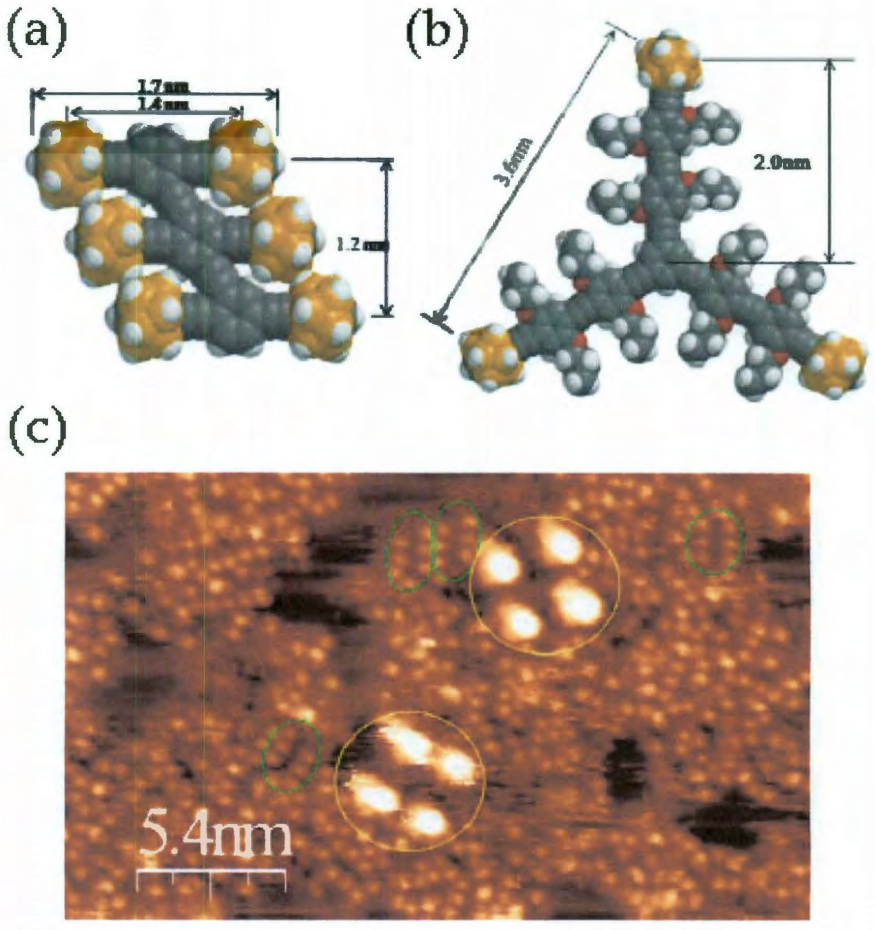

Figure 3.2: (a) The six wheeled carborane nanocar, and (b) the 3 wheeled carborane trimer molecules. In (c) carborane and C_{60} nanocars are seen on the same surface to show the size differences between the molecules. The green ovals indicate carborane nanocars and the yellow circles indicate C_{60} nanocars. Figures from [58].

fullerene, ~0.8 nm compared to ~1 nm, but the apparent height in STM is only 0.012 nm while buckminsterfullerenes have an apparent height of 0.3-0.4 nm. Despite this there were several advantages to using the carborane molecule: they are soluble in many organic solvents, they can easily be added to and substituted on the OPE chassis, and they don't adsorb light at 365 nm [53] which is critical for attaching a Feringa molecular motor [54] as seen in [55]. For more background see [55–57], as the following is a brief review from the STM side originally published in [58].

Shown in Figure 3.2, the carborane nanocar was difficult to image individually by STM but it could be seen in clusters and near step edges, and they would even align themselves into domains based on the underlying substrate orientation after annealing. Unlike the C_{60} nanocars, it was possible to image the internal structure of the carborane nanocars. No high temperature scans of the carborane nanocar were successful, and even with currents in the pico amp range the molecules were too fickle to be manipulated individually. But this leads us to the next two incarnations of the nanocar.

3.4 A New Direction

Two new classes of nanocar molecules, one featuring a completely different wheel style based on octahedral 18-electron trans-alkynylbis(1,2-bis-(diphenylphosphino) ethane)ruthenium(II) complexes, abbreviated as trans-[Ru(C≡CH)$_2$(dppe)$_2$], or simply ruthenium complexes, were synthesized by the Tour group [59]. One, the Ru nanocar, is the primary focus of Chapter 4 and will be discussed there. The other respresents a mix of carborane and C_{60} to form what was called the nano dragster (see Figure 3.3). Explored in detail in [60, 61], the most notable aspects of the nano dragster were the two different wheel units, 2 carborane wheels and 2 C_{60} wheels. The C_{60} wheel strongly adhered to the Au surface while the carboranes were much more mobile, so mobile in fact that the carboranes could pivot vertically around the C_{60} wheels, essentially "flipping" the molecule. The threshold for lateral movement appeared to be ~200 MΩ as determined by noting when the scanning conditions began to push the molecules out of the frame of view. Upon heating the surface to 77 °C the dragsters on the terraces began pivoting. Above 100 °C the dragsters showed translational motion along their chassis, but above 440 °C the motion was too fast to follow with the STM. This information is important and will be needed to compare the Ru nanocar to the previously established C_{60} nanocar family.

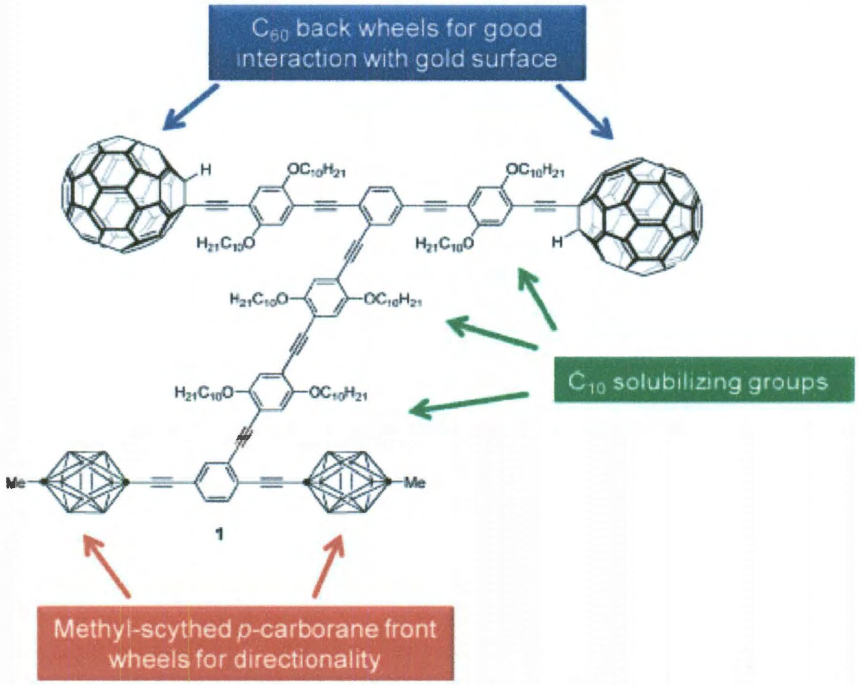

Figure 3.3: The nano dragster. Figure from [60]

Chapter 4

Ru and C_{60} Nanocars

4.1 Introduction

The ability to control components at continuingly smaller scales is one goal of nanotechnology. Small scale molecular machines that can mimic their biological brethren represent an ideal focal point for many working in the field as the investigation of nanoscale devices continues to reveal new wonders. For now scientists are working on controlling evermore complex molecules, both in solution and on surfaces, both individually and in aggregate, in the hopes of developing true molecular scale machines capable of performing predetermined tasks. The components of biological systems, such as proteins and DNA, undergo complex movements in response to external stimuli [62–64]. On surfaces, much work has been done on the manipulation of single atoms [37, 65] to form structures [31, 38], carbon nanotube movement [66], Lander molecules [67, 68], wheelbarrow molecules [39], single-wheels [40], stationary molecular rotors [69], and other larger molecules [70, 71]. The instruments used depend greatly on the type of system under study, though the principles applied should be universal. One prototype molecular machine is the nanocar, which was designed to study surface interactions as they relate to rolling and sliding [50], and the focus of this study.

Here STM tip manipulation studies were performed on nanocars deposited on an Au(111) surface at room temperature. We show the conditions required for tip induced motion, and explore how the orientation of the tip path relative to the molecule affects those conditions. In comparing the two molecules, we show that the fullerenes have a much higher activation energy and are more strongly bound to the Au sur-

face than their Ru-based counterpart. Confirming previous C_{60} nanocars studies, the molecule moves easier parallel to its chassis direction than along the axle direction [50]. The Ru-wheeled nanocars proved difficult to work with, as they were prone to degradation at high temperatures and interacted with the STM tip much more readily, which made scanning difficult.

4.2 Nanocar Molecules

The nanocar molecule [72] was developed by the Tour Group at Rice University for the purpose of exploring directed surface rolling motion [50]. The molecule (Figure 4.2) consisted of an oligo(phenylene ethynylene) (OPE) [73,74] structure with C_{60} attached at selected locations through alkynyl groups. The fullerenes were designed to freely rotate independently on the chassis and so the nanocars were ideal molecules to use for the investigation of nanoscale rolling motion. Many different types of nanocar molecules have been synthesized to date [59]. Being a somewhat modular molecule, we sought to test how changing the wheel units would affect the surface interactions. Building on older designs, we studied a new class of nanocars with organometallic Ru-based wheels [75], replacing the C_{60} from previous studies [50]. The molecules focused on here are the Ru Nanocar (RuNC) and for comparison the C_{60} Nanocar (C60NC) (Figure 4.1 & Figure 4.2)

4.3 STM Tip Manipulation

Scanning probe manipulation, first accomplished by Eigler and Schweizer [37], involves bringing the STM tip close to the target until the attractive forces between the tip and the target atom are equal to the site-to-site barrier energy [29]. The tip is then moved to a new location taking the target, trapped in the potential well, with it. At the destination the tip is withdrawn while the target stays in place due to the attraction of the surface. Complex patterns can be created out of many individual atoms on the surface [38], and even larger, more complicated molecules can be

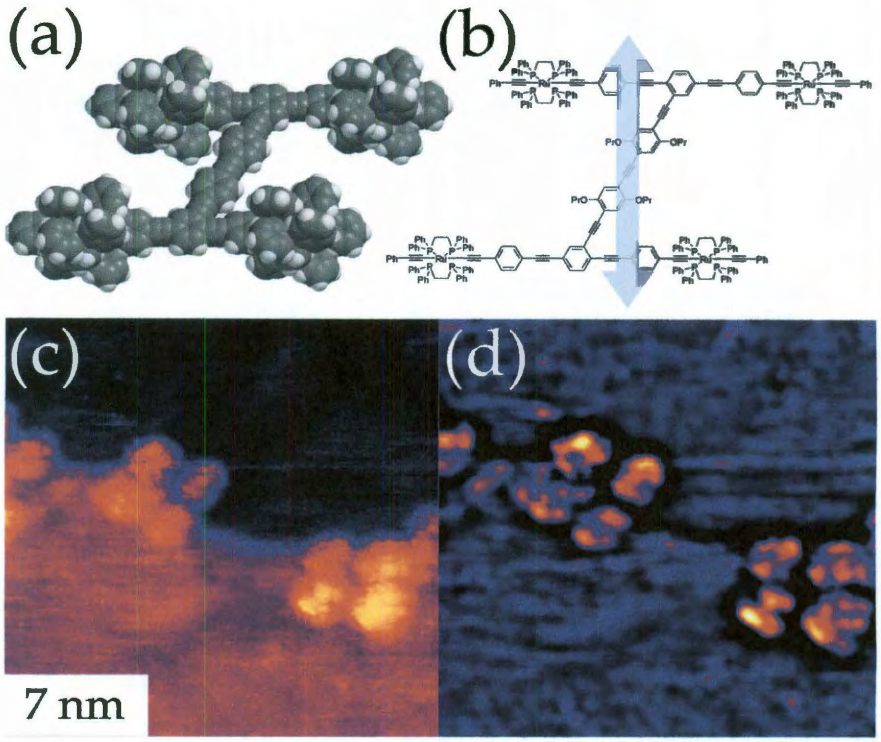

Figure 4.1: (a) shows schematic of the Ru-based nanocar. There are four Ru atoms at the center of each wheel unit, surrounded by 9 phenyl groups which are linked together by ligands. The synthesis method and structural details can be found elsewhere [75]. The RuNC showed an adsorption site preference for step-edges on the Au(111) surface at room temperature.

manipulated [39, 40]. The exact tunneling current and bias voltage required to move a molecule can tell us a lot about its interactions with the surface [31]. The gap resistance, $R_{gap} = V_{bias}/I_{tunneling}$, is the best measure of tip height as any change to the bias and current that leave the gap the same will also leave the tip height mostly unaffected [23]. By looking at the gap resistance required to move different types of molecules we can gauge their relative surface interaction strength. By recording the manipulation parameters over many attempts we can piece together a picture that tells how the molecule reacts to the tip and the type of motion that occurs. The basics are as follows: if there is a threshold voltage, above which the molecules move mostly independent of the current, then the tip is pushing/pulling due to the electric field

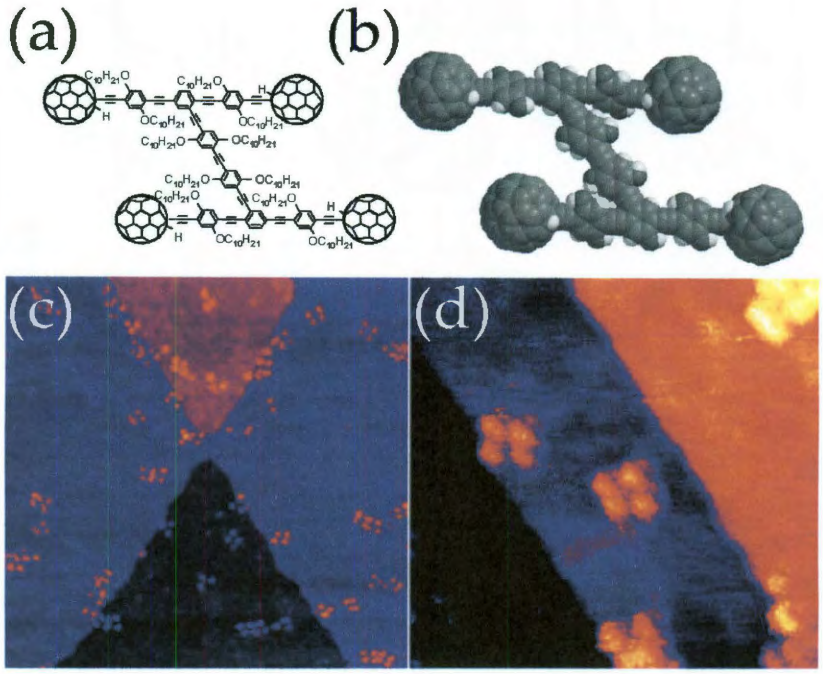

Figure 4.2: (a) C60NC molecular diagram, and (b) space filling model. (c) Numerous C_{60} nanocars deposited onto a Au(111) surface (100 nm $\times$ 100 nm). (d) Two C_{60} nanocars near a step edge (24 nm $\times$ 24 nm). Images taken at 20 pA, -0.5 V.

around the tip [33]; if there is a threshold current, above which the molecules move mostly independent of the bias voltage, then the molecules are responding to electron injection; if the there is a threshold gap resistance, above which the molecules don't respond, then the mechanism is most likely a van der Waals interaction [31, 34] and simply depends on tip distance.

One important point is that the orientation of the molecule relative to the surface lattice can have a effect on the interaction strength [29, 39, 67, 76]. We have never noticed such effects with the nanocar, possibly because of the diameter of the wheels relative to the corrugation of the Au lattice. A single nanocar occupies multiple on-top, bridge, and hollow sites. There is some evidence though that motion orientated along the Au herringbone superstructure can be recognized in the scan lines recorded during manipulation as discussed later in this chapter.

4.4 Experimental Details

The nanocars were suspended in toluene (5 μM) and sonicated for 10 min to 1 hr prior to deposition. The Au(111) [44] was purchased from Aglient[1] and cleaned through multiple cycles of sputtering and annealing with Ar^+ at 400 °C under ultra high vacuum (UHV) conditions. The solution was then dosed onto the surface through the use of a solenoid dosing valve [49,77,78] in UHV. The low decomposition temperature of the molecules (200-300 °C) ruled out the use of deposition using a sublimation technique. The sample was scanned under UHV with a base pressure of 5×10^{-10} torr at room temperature using mechanically cleaved Pt/Rd or Pt/Ir tips, purchased from Alfa Aesar[2].

Upon examination, the molecules were randomly and unevenly distributed across the surface. A much higher percentage of the Ru-based molecules preferred adsorption onto Au step edges. Multiple areas were scanned until one was found with low enough coverage under a clean Au region. Regular scanning conditions for the Ru base molecules were 1-10 pA at -0.5 V. This ensured that the tip was not interacting needlessly, as multiple scans over a single region usually resulted in no incidents of molecular movement. All bias voltages were applied to the sample unless otherwise noted.

4.5 Results and Discussion

As seen earlier in Figure 4.1, which shows a schematic of the Ru based nanocar, there is a Ru atom at the center of each wheel unit, surrounded by 9 phenyl groups which are linked together by ligands. The synthesis method and structural details can be found elsewhere [59]. The RuNC showed an adsorption site preference for step-edges

[1]Agilent Technologies Gold-coated substrates with 1500 Å Au (111) Covering 2.0 cm × 2.1 cm; cut to ~0.5 cm × 0.5 cm to fit sample holders.

[2]80% Platinum wire with 20% Rhodium by weight, 0.25 mm diameter, typically 1 m long, and cut for use to ~0.6 mm

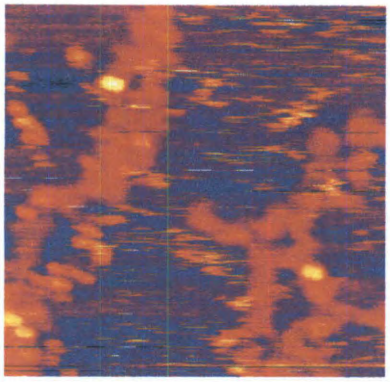

Figure 4.3: RuNCs at elevated temperatures (T=42 °C), showings streaks and blurs indicating motion on a time scale faster than the STM acquisition time. The image size is 70 nm x 70 nm.

on the Au(111) surface (Figure 4.1b). In one sense the molecule has more binding sites available and can lower its potential energy at the edges, as opposed to the terraces. The Ru molecules can be imaged similar to the previous C60NC studied [50], showing four large lobes without any internal OPE structure [79]. Care must be taken to ensure that the complex under observation is actually a cohesive molecule and not a random grouping of four loose ruthenium complexes. A manipulation attempt can be one measure to test cohesiveness, as can repeatedly scanning the area and watching for any motion; single ruthenium complexes are less stable in adsorption sites than the full nanocar.

C_{60} molecules on Au do not readily show their intermolecular structure, but it is possible to resolve under clean environments [80]. Likewise, the phenyl groups on the RuNC do not show themselves under normal scanning conditions (10-20 pA, -0.05-1 V), but using high pass filtering it is possible to pullout out the corrugation details of the wheels in such images. Figure 4.1(d) shows an image of the RuNC on a step-edge after highpass filtering. By observing such internal structure, one can monitor the wheel conditions as the molecules translate across the surface.

Because the RuNC were stable at room temperature in UHV conditions, we attempted to measure their motion at elevated temperature. It quickly became apparent that the molecules were mobile and chemically unstable above 40 °C, as the images showed streaking and dismantled pieces of the molecules. The streaking in Figure 4.3

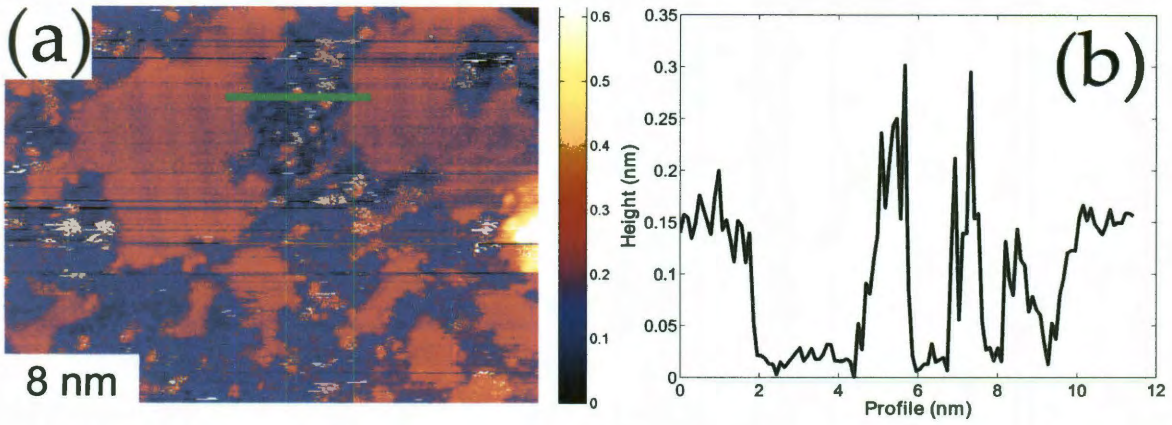

Figure 4.4: RuNC sample after heating to T=170 °C. In (a) there are higher and lower regions, with the higher regions showing the herringbone structure. The green line indicates the path of the profile shown in (b). The raised regions are about 0.15 nm higher, with some feature reaching 0.3 nm in height compared to the lower background. Scanning conditions were 9 pA, -0.5 V, 55.5 GΩ.

indicates motion on a timescale that is faster than the STM acquisition time. Figure 4.4a shows an image taken after the substrate was heated to 170 °C. The surface appeared covered by islands, similar to benzene on Au(111) [81], with the herringbone structure visible through the suspected phenyl overlayer caused by the breakdown of the RuNCs. The high mobility of the islands at high temperature prevented any molecular level resolution, obfuscating the exact overlayer structure. It is thought that the Au acts as a catalyst for the RuNC dissociation which in solution is stable up to 300 °C [75]. For comparison, the C_{60} based nanocars could be readily imaged, with motion discernible, at high temperatures around 200 °C [50]. Temperatures from 50 to 200 °C were tested for observable RuNC motions, but none were found. The molecules appeared to be stable at room-temperature on step-edges, but aggressive tunneling parameters would removing them from their potential well, or grab onto them resulting in a loss of imaging capability which could be recovered by zapping or crashing the tip on Au. As of yet, no above room temperatures scans of the RuNC molecule have been successfully performed.

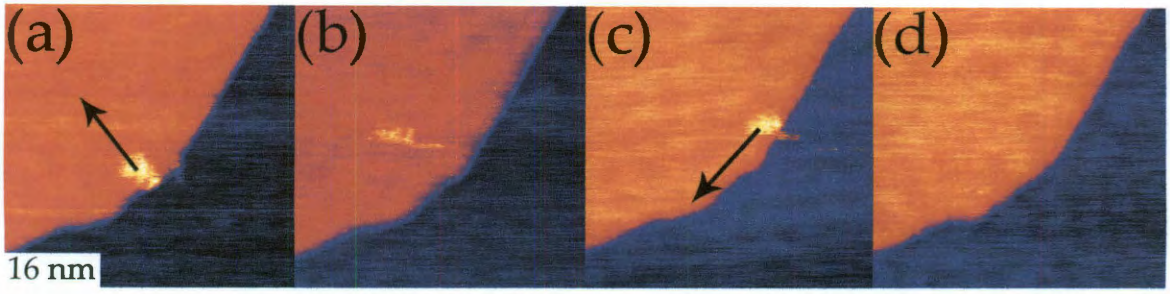

Figure 4.5: (a) Image of a RuNC on a step-edge, and the motion of the tip during a manipulation event. (b) Shows the molecule having moved ~15 nm, while the tip itself moved 20 nm. The molecule also shows some streaks, which indicate motion under the tip. About 8 minutes passed between these two scans. (c) ~1 min later, the molecules had moved back to the step-edge, where another manipulation attempt is performed, and this time along the step-edge. (d) After the event the molecule is no longer in the field of view. 48 nm × 48 nm, scanning conditions were 10 pA, -0.5 V, 50 GΩ, manipulation conditions were 400 pA, -50 mV, 100 MΩ.

When stable Ru nanocar molecules were found at room-temperature we attempted to manipulate them with the STM tip. Many manipulation attempts took place near step-edges, where the molecules preferentially adsorbed, and the resulting motion then brought the molecules onto the terraces or farther along the step-edge. Here, in Figure 4.5a, after imaging at 10 pA and -0.5 V the tip was placed above the molecule, lowered (increasing the tunneling current to 400 pA and decreasing the voltage to -0.05 V), then moved towards the upper left at 5 nm/s over a distance of 20 nm. Afterwards, a second scan was done with the tip farther from the surface showing the motion that occurred. In Figure 4.5b the RuNC is about ~15 nm from the step-edge and is stable enough to be imaged, though it is possible to see a tail, or streak, on the bottom right edge of the molecule. As the tip scans from top to bottom, this streak indicates that some motion occurred as the tip was nearing the bottom of the molecule, and so perhaps the molecule moved from the position it was occupying at the start of the scan. This is confirmed in Figure 4.5c, which shows the RuNC back against the Au step-edge, a more stable position for it. Again, a tip manipulation was attempted, this time though along the direction of the step-edge (to the bottom

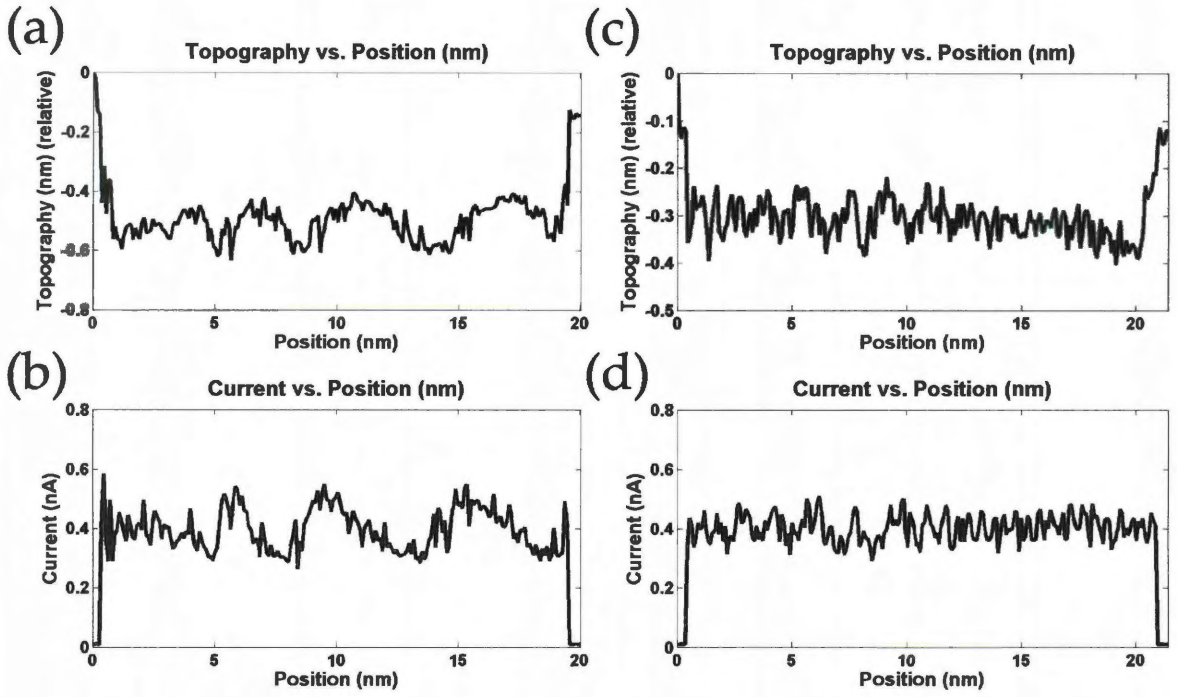

Figure 4.6: (a) & (b) show the topographic and current curves taken during the manipulation event shown in Figure 4.5(a) and (b). (c) & (d) show the curves for the second manipulation event shown in Figure 4.5(c) and (d).

left) with the same conditions as before. The following image showed no RuNC in the expected area though. As the molecules have no practical momentum due to their size, it is likely the tip jettisoned the molecule out of the field of view, rather than the molecule continuing to slide along the step-edge [82], though with gentle conditions the RuNCs would jump around the terraces at room temperature.

The manipulation curves taken during the first and second events are displayed in Figure 4.6. That the curves do not readily correspond to those presented in previous work [29, 31, 40, 66, 83] is not as odd as it first seems as it is speculated that the complexity of the molecule [70, 71], and the fact that at room temperature the RuNC are close to escaping their local potential wells, results in the more obscure signals seen here. There do seem to be differences between the two translational directions as well, with the signal from the lateral motion orthogonal to the step-edge boundary

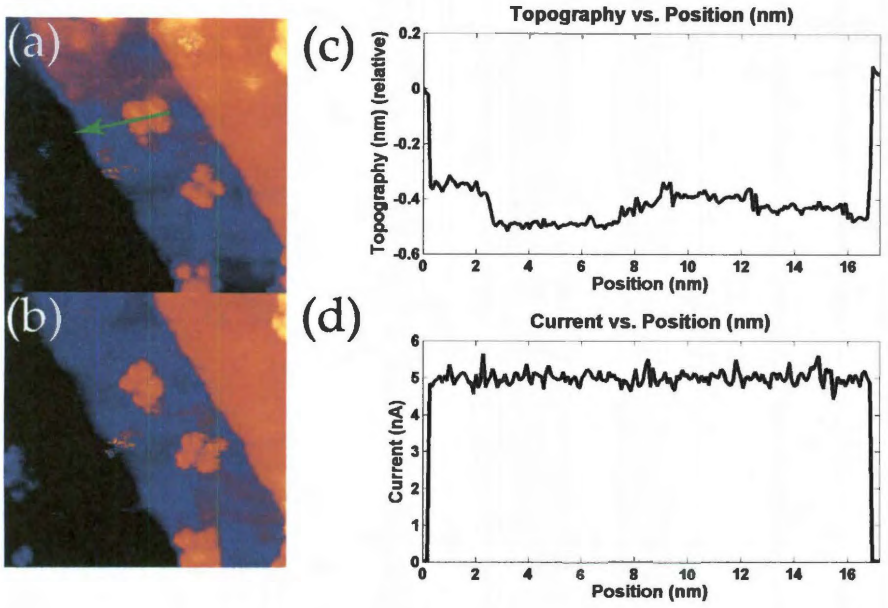

Figure 4.7: (a) A manipulation attempt on a C60NC parallel to the axles. (b) The molecule is shifted slightly, but does not move from its original location. The manipulation conditions were -50 mV, 5 nA, 10 MΩ. The image size is 34.7 nm × 34.7 nm. Scanning conditions were -0.5 V, 20 pA. The topographic line scans (c) and current line scans (d) show few features.

having a well defined oscillation, while the signal from the motion parallel to the step-edge has some oscillation but with a much higher frequency.

The C60NC could be manipulated easily on terraces or step-edges, or moved in a controlled fashion from one to the other with the STM tip. Figure 4.2(c) & (d) show several images of C60NC's on step-edges and terraces on the Au(111) surface. Again, the fullerene wheels are readily visible, but the internal OPE structure is not. No scans to date of this particular nanocar have revealed the internal structure. Figure 4.7(a) shows the setup for a manipulation attempt on a C60NC molecule near a step-edge. Notice that the motion of the tip is parallel to the axles, and hence this motion will not cause the wheels to rotate. From previous work on C60NC [50], tip motions parallel to the axles did not induce motion, so we expect for the molecule to remain stationary here. The current is increased from 20 pA to 5 nA, and the bias

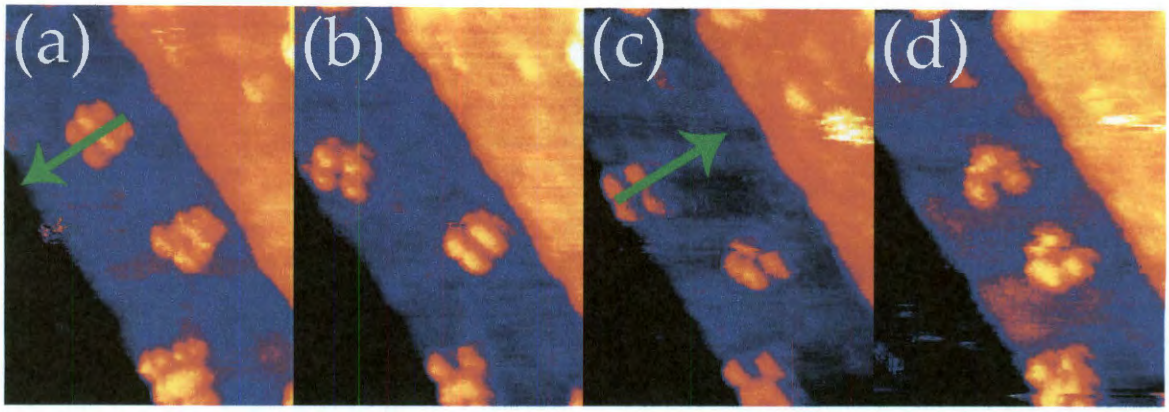

Figure 4.8: (a) The tip is brought close to the nanocar and, perpendicular to the axels, is moved towards the step-edge. (b) The next scan shows the successful movement. (c) A later scan shows the nanocar has rotated on its own to align with the step-edge, and for a second time the tip is brought close to the nanocar, perpendicular to the axles, and moved away from the step-edge. Image (d) shows the results of the successful manipulation and the final placement of the nanocar. Image size is 25 nm $\times$ 35 nm. Manipulation conditions were -50 mV, 6 nA, 8.3 MΩ. Scanning conditions were -0.5 V, 20 pA.

decreased from -0.5 V to -50 mV, which gives gap resistances spanning 25 GΩ to 10 MΩ ($\sim$3 orders of magnitude). Looking at Figure 4.7(b), taken after the manipulation attempt, the molecule is still in the same location, though rotated slightly. Before in Figure 4.7(a) the axles were perpendicular to the step, but in Figure 4.7(b) they have rotated to be parallel to the step-edge. Looking at the topographic and current scan lines in Figure 4.7(c) and (d) shows a step after the tip has traveled $\sim$2 nm in the topography. This is first part is the tip moving over the molecule, but when it doesn't follow the tip moves closer to the surface to maintain the current set-point. The height of the C60NC from the topographic line is only $\sim$2 Å, compared to the normal C_{60} apparent height of 3-4 Å [84, 85]. As the tip is not passing over the center of the C_{60} structure there is no real discrepancy here. Figure 4.8(a) picks up where Figure 4.7(b) leaves off and is the start of a second manipulation attempt on this molecule, now perpendicular to the axles. The successful results are shown in Figure 4.8(b). Between (b) and (c) the nanocar rotated slightly to align its axles with the step-edge.

Whether this was the result of tip interactions while scanning or simply the molecule settling into a lower potential is unknown, but given the scanning conditions (20 pA, -0.5 V, 25 GΩ) there should be little to no tip/molecule interactions [43]. While, we do not know the orientation of the C_{60} wheel relative to the Au, several papers have explored how clusters of C_{60} adsorb on Au(111) [80, 86–89] and the importance of step-edges for C_{60} adsorption and cluster nucleation [43]. Neither image shows any streaks or blurs around the nanocar, as the RuNC did in Figure 4.5(b) when it was shifting positions during the scan. It is probable that the nanocar shifted to align itself with the step-edge on its own, without the interference of the tip. In 4.8(c) the tip is brought close to the nanocar again and moved away from the step-edge. In subset (d) of Figure 4.8 shows the final position of the molecule, after having been moved away from the step-edge by the tip. The C60NC is a dynamic molecule, and these lateral manipulations studies show the importance of the alignment of tip and axle for induced surface motion.

One interesting case is when the gap resistance is brought too low and the tip does irreversible damage to the molecule. Instead of the molecule/tip interaction being attractive and equal to the lateral potential well, it moves into the repulsive regime. It is interesting that in many of these cases the molecule does not zip off in some direction as a whole but instead will crumple, with 1 or more wheels detaching or contorting while part of the molecule remains in place, or the tip will leave detritus along its path. One possible example of the former is shown in Figure 4.9, where the manipulation conditions were 6 nA and 50 mV (8.3 MΩ). Two previous attempts at 4 nA & 50 mV (12.5 MΩ) had not resulted in any motion. Two 6 nA attempts were then made at the same bias, and on the second attempt the molecule contorted. The center-to-center spacings of the C_{60} molecules in an intact car are 3.11 nm along the axle and 1.98 nm along the chassis, though due to the flexibility of the OPE chassis there is some variability [52]. Before manipulation (Figure 4.9a) this particular molecule had center-to-center spacings, along the lines defined in the insert of Figure 4.9a, of

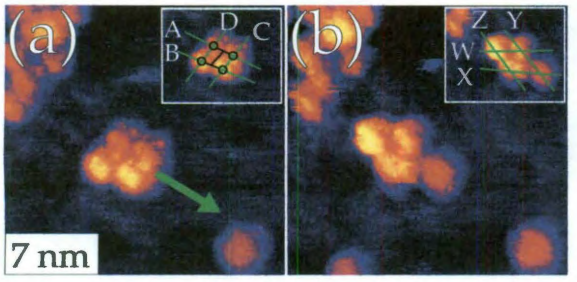

Figure 4.9: STM tip manipulation of a C_{60} nanocar. (a) Before image showing the target molecule. (b) After the manipulation event the molecule was destroyed. Manipulation conditions were 6 nA, -50 mV, 8.3 MΩ, 5 nm/s tip speed. Images taken at 20 pA, -0.5 V.

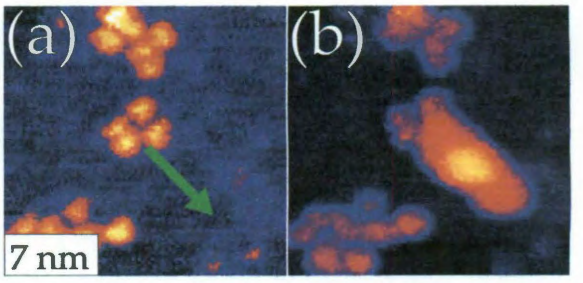

Figure 4.10: Before (a) and after (b) of a failed tip manipulation where physical damage was done to the sample. Manipulation conditions were 8 nA, -25 mV, 3.13 MΩ. Images taken a 20 pA, -0.5 V.

A: 2.51 nm, B: 2.35 nm, C: 1.77 nm, and D: 1.96 nm. The manipulation direction was parallel to the axles (along A & B, see insert overlay) and attempted to move the molecule perpendicular to its normal direction of motion. After the manipulation attempt the center-to-center spacing along the lines defined in Figure 4.9b insert were W:2.70 nm, X: 3.35 nm, Y: 3.81 nm, and Z: 2.87 nm. The displacement of the lower right wheel in Figure 4.9b (intersection of lines X & Y) is either caused by stretching an axle, or by the rotation of the OPE chassis, or both depending on the orientation of the nanocar after the tip manipulation. In [52](See Figure 3.5 caption, and Chapter 5) it was noted that "Front and rear fullerenes on the same side of a molecule can show a large discrepancy in peak to peak distance measurements, while fullerenes along an axle maintain a much smaller range of measurements." Basically, the distance between two C_{60} molecules along an axle is unlikely to change and so any large discrepancies in C_{60} placement are more likely to arise from a buckling or bending of the OPE chassis. From this we infer that we largest center-to-center distance, line Y in Figure 4.9b, is along the chassis direction, while lines W and X are along the two axles. The increases in length after manipulation are summarized in Table 4.1.

Table 4.1: Center-to-center C_{60} distance in nm from Figure 4.9

	Theoretical	Before	After
Axle	3.11	A: 2.51	W:2.70
		B: 2.35	X: 3.35
Chassis	1.98	C: 1.96	Y: 2.87
		D: 1.77	Z: 3.81

It is possible that the fullerene was ripped off the axle, but single fullerenes diffuse rapidly on Au(111) [43] and are not visible on STM scan timescales. Though 6 nA was on the high side of the amount of current required for lateral movement, several other C60NCs had been successfully moved with similar conditions. Multiple scans showed no streaking or blurring, and the previous manipulation attempts did not dislodge any of the C_{60} wheels. Similarly, in Figure 4.10, a manipulation attempt along the chassis (preferred direction) with a gap resistance of 3.13 MΩ actually damaged the surface. It is possible that material from the tip was transfer to the surface, given the protrusion along the path of the tip. In such cases the nanocar can no longer be used for tip manipulation studies as it has effectively been destroyed.

To gain more insight into the nature of the nanocar surface interaction we performed a number of manipulation events on RuNCs (N_{Ru}=50) and C60NC ($N_{C_{60}}$=77) and recorded the parameters. The average gap resistance for successful tip manipulation for the RuNCs was 191 MΩ, while the gap for the C60NCs was 21 MΩ. This confirms previous studies [50] of the C60NC where a successful tip manipulation was achieved with 28.5 MΩ. The fact that the gap resistance for the RuNCs was an order of magnitude higher than the C60NC means that it interacts with the tip from a much greater distance than the C60NC. The van der Waals force [34] drops off as $1/r^{-6}$, so the RuNC site potential for lateral movement is much lower than that for the C60NC. This confirms our earlier high temperature studies where the C60NCs were stable and imaged at high temperatures while the RuNCs were unstable at temperatures above 50 °C (Figure 4.3).

4.6 Conclusion

The different types of nanocars all show how the molecular/surface interaction changes with differing functionalization of the wheel units. Simply put, the C_{60} units provide the most stable interaction with the Au(111) surface, which is unfortunate as they are the most arduous to synthesize. By mixing C_{60}/carborane wheels the surface interaction is decreased and the molecules move with a lower gap resistance and with less thermal energy, while a wholly carborane nanocar is diffusing at room temperature unless stabilized by clusters (see Chapter 3). Here the new Ru nanocar takes the middle ground and displays room temperature stability. Much like the carborane nanocars though, it quickly reaches its threshold energy and diffuses above 50 °C. Additionally, these studies confirm that the OPE axles possess a very small barrier to rotation as expected and that the strength of the molecule surface interaction can be readily tuned by the appropriate choice of wheel molecule and surface. In learning about the way different fullerene like molecules interact with surfaces we can prepare the chemical ingredients for capable and efficient molecular machines.

Chapter 5

Conclusion

This work explored how fullerene and fullerene-like molecules attached to a semi-rigid OPE chassis move on an Au(111) surface at room temperature and above, as well as the threshold resistance required to laterally translate these molecules across the substrate. The weakly interacting carborane molecules exhibited the lowest thermal threshold, being stable only in clusters on the surface, never individually. The Ru-based nanocar moved erratically and degraded above 50 °C, while the mixed wheeled dragster showed rotational movement at 70 °C and translational at 100 °C. The C_{60} nanocar was the most stable and could be imaged from 170 °C to 300 °C. The difficulty and time required to actually synthesize these molecules sadly increases in this same order, making future applications of this particular nanocars unlikely, but the knowledge gained will undoubtedly influence future work in molecular machines. The concepts themselves are extraordinary, both for their possible application to the myriad of technologies that utilize surface chemistry and their ability to unlock areas of science that remain yet unexplored. As we continue to investigate more complex nanoscale systems the application of fundamental mathematical physics becomes more and more time consuming, where even now many of the experiments preformed are too complex to model accurately without approximations. This means experimentalists will have to build and test these systems if we want data from them in the near future.

Continuing work on the nanocar project involves a variety of idea now, some of which are: depositing salt and metal island on the Au(111) substrate which would change the interaction and either "speed up" or "slow down" the nanocar motion at high temperatures, depending on the charge transfer and chemical bonding strength;

attaching thiol groups to the carborane molecules as in [90,91] to anchor the carborane nanocars; and electric field gradients across the sample to directionally orient all the molecules on the surface.

Hopefully this work has provided something back to the scientific fields which have given so much knowledge to the rest of us.

Bibliography

[1] M. P. Marder, *Condensed Matter Physics.* Wiley-Interscience, 1 ed., Jan. 2000.

[2] I. Giaever, "Electron tunneling and superconductivity," *Reviews of Modern Physics*, vol. 46, p. 245, Apr. 1974.

[3] W. A. Thompson and S. F. Hanrahan, "Thermal drive apparatus for direct vacuum tunneling experiments," *Review of Scientific Instruments*, vol. 47, no. 10, p. 1303, 1976.

[4] G. Binnig and H. Rohrer, "Scanning Tunneling Microscopy–'from Birth to Adolescence (Nobel Lecture)'," *Angewandte Chemie International Edition in English*, vol. 26, no. 7, pp. 606–614, 1987.

[5] J. Curie and P. Curie, "Sur lelectricite polaire dans les cristaux hgmiedres faces inclinees," *Comptes Rendus*, vol. 91, pp. 383–386, 1880.

[6] G. Lippmann, "Principe de la conservation de l'electricitea ou second principe de la theorie des phenomnes electriques," *J. de Phys.*, vol. 10, pp. 381–394, 1881.

[7] J. Curie and P. Curie, "Deformations electriques du quartz," *Comptes Rendus*, vol. 95, pp. 914–917, 1882.

[8] G. Binnig, H. Rohrer, C. Gerber, and E. Weibel, "Surface studies by scanning tunneling microscopy," *Physical Review Letters*, vol. 49, p. 57, July 1982.

[9] C. Davisson and L. H. Germer, "Diffraction of electrons by a crystal of nickel," *Physical Review*, vol. 30, p. 705, Dec. 1927.

[10] R. J. Culbertson, L. C. Feldman, and P. J. Silverman, "Atomic displacements in the Si(111)-(7x7) surface," *Physical Review Letters*, vol. 45, p. 2043, Dec. 1980.

[11] D. E. Eastman, "Geometrical and electronic structure of Si(001) and Si(111) surfaces: A status report," *Journal of Vacuum Science and Technology*, vol. 17, no. 1, p. 492, 1980.

[12] N. Garcia, "The surface profile of charge of Si(111)(7x7) obtained with he scattering," *Solid State Communications*, vol. 40, no. 7, pp. 719 – 723, 1981.

[13] F. J. Himpsel, D. E. Eastman, P. Heimann, B. Reihl, C. W. White, and D. M. Zehner, "Electronic structure of the annealed Ge(111) and Si(111) surfaces: Similarities in local bonding," *Physical Review B*, vol. 24, p. 1120, July 1981.

[14] C. Su, P. Skeath, I. Lindau, and W. Spicer, "The nature of the 7x7 reconstruction of Si(111): As revealed by changes in oxygen sorption from 2x1 to 7x7," *Surface Science*, vol. 107, no. 2-3, pp. L355 – L361, 1981.

[15] L. C. Snyder, "Milk-stool model for Si(111) surface reconstruction," *Journal of Vacuum Science and Technology*, vol. 16, no. 5, p. 1266, 1979.

[16] J. Pollmann, "New hexagonal ring model for the reconstruction of the Si(111)-7x7 surface," *Physical Review Letters*, vol. 49, p. 1649, Nov. 1982.

[17] J. C. Phillips, "New model for reconstructed Si(111) 7x7 surface superlattices," *Physical Review Letters*, vol. 45, no. 11, p. 905, 1980.

[18] G. L. Lay, "New model for the reconstructed Si(111)7x7 and Si(111)$\sqrt{19}$x$\sqrt{19}$-R($\pm$23°5) surfaces," *Surface Science*, vol. 108, no. 1, pp. L429 – L433, 1981.

[19] G. Binnig, H. Rohrer, C. Gerber, and E. Weibel, "7x7 reconstruction on Si(111) resolved in real space," *Physical Review Letters*, vol. 50, p. 120, Jan. 1983.

[20] K. Takayanagi, Y. Tanishiro, S. Takahashi, and M. Takahashi, "Structure analysis of Si(111)-7x7 reconstructed surface by transmission electron diffraction," *Surface Science*, vol. 164, no. 2-3, pp. 367 – 392, 1985.

[21] "The Nobel Prize in Physics 1986". Nobelprize.org. 5 Oct 2010 `http://nobelprize.org/nobel_prizes/physics/laureates/1986/`.

[22] "LEED | surface physics group, university of york." `http://www-users.york.ac.uk/~phys24/Pages/Techniques/LEED/`.

[23] C. J. Chen, *Introduction to Scanning Tunneling Microscopy.* Oxford University Press, USA, 2 ed., Dec. 2007.

[24] J. Bardeen, "Tunnelling from a Many-Particle point of view," *Physical Review Letters*, vol. 6, p. 57, Jan. 1961.

[25] R. Wiesendanger, *Scanning Probe Microscopy and Spectroscopy: Methods and Applications.* Cambridge University Press, Nov. 1994.

[26] F. London, "Zur theorie und systematik der molecularkräfte," *Zeits. f. Physik*, vol. 63, pp. 245–258, 1930.

[27] L. D. Landau and L. M. Lifshitz, *Quantum Mechanics Non-Relativistic Theory, Third Edition: Volume 3.* Butterworth-Heinemann, 3 ed., Jan. 1981.

[28] J. A. Stroscio and D. M. Eigler, "Atomic and molecular manipulation with the scanning tunneling microscope," *Science*, vol. 254, pp. 1319–1326, Nov. 1991.

[29] H. Tang, "Fundamental considerations in the manipulation of a single C_{60} molecule on a surface with an STM," *Surface Science*, vol. 386, no. 1-3, pp. 115–123, 1997.

[30] J. A. Stroscio and R. J. Celotta, "Controlling the dynamics of a single atom in lateral atom manipulation," *Science*, vol. 306, no. 5694, pp. 242–247, 2004.

[31] S. Hla, K. Braun, and K. Rieder, "Single-atom manipulation mechanisms during a quantum corral construction," *Physical Review B*, vol. 67, no. 20, 2003.

[32] C. J. Chen, "A universal relation in NC-AFM, STM, and atom manipulation," *Nanotechnology*, vol. 16, no. 3, pp. S27–S34, 2005.

[33] M. Ohara, Y. Kim, and M. Kawai, "Electric field response of a vibrationally excited molecule in an STM junction," *Physical Review B*, vol. 78, no. 20, 2008.

[34] H. Hamaker, "The london–van der waals attraction between spherical particles," *Physica*, vol. 4, pp. 1058–1072, Oct. 1937.

[35] R. S. Becker, J. A. Golovchenko, and B. S. Swartzentruber, "Atomic-scale surface modifications using a tunnelling microscope," *Nature*, vol. 325, pp. 419–421, Jan. 1987.

[36] J. S. Foster, J. E. Frommer, and P. C. Arnett, "Molecular manipulation using a tunnelling microscope," *Nature*, vol. 331, pp. 324–326, Jan. 1988.

[37] D. M. Eigler and E. K. Schweizer, "Positioning single atoms with a scanning tunneling microscope," *Nature*, vol. 344, p. 524, Apr. 1990.

[38] M. F. Crommie, C. P. Lutz, D. M. Eigler, and E. J. Heller, "Quantum corrals," *Physica D: Nonlinear Phenomena*, vol. 83, pp. 98–108, May 1995.

[39] L. Grill, K. H. Rieder, F. Moresco, G. Jimenez-Bueno, C. Wang, G. Rapenne, and C. Joachim, "Imaging of a molecular wheelbarrow by scanning tunneling microscopy," *Surface Science*, vol. 584, no. 2-3, p. 153158, 2005.

[40] L. Grill, K. Rieder, F. Moresco, G. Rapenne, S. Stojkovic, X. Bouju, and C. Joachim, "Rolling a single molecular wheel at the atomic scale," *Nature Nanotechnology*, vol. 2, no. 2, pp. 95–98, 2007.

[41] M. H. Hablanian, *High-Vacuum Technology.* Marcel Dekker Inc, 2 ed., Mar. 1997.

[42] K. Besocke, "An easily operable scanning tunneling microscope," *Surface Science*, vol. 181, pp. 145–153, Mar. 1987.

[43] S. Guo, D. P. Fogarty, P. M. Nagel, and S. A. Kandel, "Thermal diffusion of C_{60} molecules and clusters on Au(111)," *The Journal of Physical Chemistry B*, vol. 108, no. 37, pp. 14074–14081, 2004.

[44] J. V. Barth, H. Brune, G. Ertl, and R. J. Behm, "Scanning tunneling microscopy observations on the reconstructed Au(111) surface: Atomic structure, long-range superstructure, rotational domains, and surface defects," *Physical Review B*, vol. 42, p. 9307, Nov. 1990.

[45] V. M. Hallmark, S. Chiang, J. F. Rabolt, J. D. Swalen, and R. J. Wilson, "Observation of atomic corrugation on Au(111) by scanning tunneling microscopy," *Physical Review Letters*, vol. 59, p. 2879, Dec. 1987.

[46] "Agilent | hydrogen flame annealing." `http://www.home.agilent.com/agilent/editorial.jspx?cc=US&lc=eng&ckey=914989&nid=-33980.914271.00&id=914989`.

[47] C. Wöll, S. Chiang, R. J. Wilson, and P. H. Lippel, "Determination of atom positions at stacking-fault dislocations on Au(111) by scanning tunneling microscopy," *Phys. Rev. B*, vol. 39, pp. 7988–7991, Apr 1989.

[48] T. Kanno, H. Tanaka, T. Nakamura, H. Tabata, and T. Kawai, "Real space observation of Double-Helix DNA structure using a low temperature scanning tunneling microscopy," *Japanese Journal of Applied Physics*, vol. 38, pp. L606–L607, 1999.

[49] Y. Terada, B. Choi, S. Heike, M. Fujimori, and T. Hashizume, "Placing conducting polymers onto a H-terminated Si(100) surface via a pulse valve," *Nano Letters*, vol. 3, no. 4, pp. 527–531, 2003.

[50] Y. Shirai, A. J. Osgood, Y. Zhao, K. F. Kelly, and J. M. Tour, "Directional control in thermally driven Single-Molecule nanocars," *Nano Letters*, vol. 5, no. 11, pp. 2330–2334, 2005.

[51] A. J. Osgood, "Investigation and manipulation of new fullerene derivative molecules by scanning tunneling microscopy," Master's thesis, Rice University, Houston, TX, May 2005.

[52] A. J. Osgood, *Probing Molecular Adsorption and Mechanics at the Atomic Scale: The Nanocar Family of Molecules.* PhD thesis, Rice University, Houston, TX, Feb. 2008.

[53] H. Kunkely and A. Vogler, "Is o-carborane photoluminescent?," *Inorganica Chimica Acta*, vol. 357, pp. 4607–4609, Dec. 2004.

[54] R. A. van Delden, M. K. J. ter Wiel, M. M. Pollard, J. Vicario, N. Koumura, and B. L. Feringa, "Unidirectional molecular motor on a gold surface," *Nature*, vol. 437, pp. 1337–1340, Oct. 2005.

[55] J. Morin, Y. Shirai, and J. M. Tour, "En route to a motorized nanocar," *Organic Letters*, vol. 8, pp. 1713–1716, Apr. 2006.

[56] Y. Shirai, J. Morin, T. Sasaki, J. M. Guerrero, and J. M. Tour, "Recent progress on nanovehicles," *Chemical Society Reviews*, vol. 35, no. 11, p. 1043, 2006.

[57] S. Khatua, J. M. Guerrero, K. Claytor, G. Vives, A. B. Kolomeisky, J. M. Tour, and S. Link, "Micrometer-Scale translation and monitoring of individual nanocars on glass," *ACS Nano*, vol. 3, no. 2, pp. 351–356, 2009.

[58] J. Zhang, *Studying Photonic Excitations of Carborane and Fullerene Nanomachines by Probe Microscopy.* PhD thesis, Rice University, Houston, TX, Jan. 2009.

[59] G. Vives and J. M. Tour, "Synthesis of Single-Molecule nanocars," *Accounts of Chemical Research*, vol. 42, no. 3, pp. 473–487, 2009.

[60] G. Vives, J. Kang, K. F. Kelly, and J. M. Tour, "Molecular machinery: Synthesis of a nanodragster," *Organic Letters*, vol. 11, pp. 5602–5605, Dec. 2009.

[61] J. Kang, *Investigation of Graphitic Nanostructures and Nanomachines.* PhD thesis, Rice University, Houston, TX, June 2010.

[62] J. Lehn, "Perspectives in supramolecular Chemistry—From molecular recognition towards molecular information processing and Self-Organization," *Angewandte Chemie International Edition in English*, vol. 29, pp. 1304–1319, Nov. 1990.

[63] N. C. Seeman, "From genes to machines: DNA nanomechanical devices," *Trends in Biochemical Sciences*, vol. 30, pp. 119–125, Mar. 2005.

[64] Z. Wang, J. Elbaz, and I. Willner, "DNA machines: Bipedal walker and stepper," *Nano Letters*, vol. 11, pp. 304–309, Jan. 2011.

[65] G. Meyer, B. Neu, and K. H. Rieder, "Controlled lateral manipulation of single molecules with the scanning tunneling microscope," *Applied Physics A: Materials Science & Processing*, vol. 60, pp. 343–345, Mar. 1995.

[66] K. Miura, T. Takagi, S. Kamiya, T. Sahashi, and M. Yamauchi, "Natural rolling of zigzag multiwalled carbon nanotubes on graphite," *Nano Letters*, vol. 1, no. 3, pp. 161–163, 2001.

[67] R. Otero, F. Hmmelink, F. Sato, S. B. Legoas, P. Thostrup, E. Lgsgaard, I. Stensgaard, D. S. Galvo, and F. Besenbacher, "Lock-and-key effect in the surface

diffusion of large organic molecules probed by STM," *Nature Materials*, vol. 3, no. 11, pp. 779–782, 2004.

[68] S. Godlewski, G. Goryl, A. Gourdon, J. J. Kolodziej, B. Such, and M. Szymonski, "Internal architecture and adsorption sites of violet lander molecules assembled on native and KBr-Passivated InSb(001) surfaces," *ChemPhysChem*, vol. 10, no. 12, pp. 2026–2033, 2009.

[69] L. Gao, Q. Liu, Y. Zhang, N. Jiang, H. Zhang, Z. Cheng, W. Qiu, S. Du, Y. Liu, W. Hofer, and H. Gao, "Constructing an array of anchored Single-Molecule rotors on gold surfaces," *Physical Review Letters*, vol. 101, no. 19, 2008.

[70] F. Moresco, G. Meyer, K. Rieder, H. Tang, A. Gourdon, and C. Joachim, "Recording intramolecular mechanics during the manipulation of a large molecule," *Physical Review Letters*, vol. 87, no. 8, 2001.

[71] F. Moresco, G. Meyer, K. Rieder, H. Tang, A. Gourdon, and C. Joachim, "Low temperature manipulation of big molecules in constant height mode," *Applied Physics Letters*, vol. 78, no. 3, p. 306, 2001.

[72] Y. Shirai, A. J. Osgood, Y. Zhao, Y. Yao, L. Saudan, H. Yang, C. Yu-Hung, L. B. Alemany, T. Sasaki, J. F. Morin, *et al.*, "Surface-rolling molecules," *J. Am. Chem. Soc*, vol. 128, no. 14, p. 48544864, 2006.

[73] G. Jeschke, M. Sajid, M. Schulte, N. Ramezanian, A. Volkov, H. Zimmermann, and A. Godt, "Flexibility of Shape-Persistent molecular building blocks composed of p-phenylene and ethynylene units," *Journal of the American Chemical Society*, vol. 132, pp. 10107–10117, July 2010.

[74] A. Villares, D. P. Lydon, B. J. Robinson, G. J. Ashwell, F. M. Royo, P. J. Low, and P. Cea, "Langmuir-Blodgett films incorporating molecular wire candidates of ester-substituted oligo(phenylene-ethynylene) derivatives," *Surface Science*, vol. 602, pp. 3683–3687, Dec. 2008.

[75] G. Vives and J. M. Tour, "Synthesis of a nanocar with organometallic wheels," *Tetrahedron Letters*, vol. 50, no. 13, p. 14271430, 2009.

[76] D. Y. Zhong, J. Franke, T. Blomker, G. Erker, L. F. Chi, and H. Fuchs, "Manipulating surface diffusion ability of single molecules by scanning tunneling microscopy," *Nano Letters*, vol. 9, no. 1, pp. 132–136, 2009.

[77] L. Grill, I. Stass, K. H. Rieder, and F. Moresco, "Preparation of self-ordered molecular layers by pulse injection," *Surface Science*, vol. 600, no. 11, p. 143147, 2006.

[78] H. Tanaka and T. Kawai, "Partial sequencing of a single DNA molecule with a scanning tunnelling microscope," *Nature Nanotechnology*, vol. 4, no. 8, pp. 518–522, 2009.

[79] R. Magyar, S. Tretiak, Y. Gao, H. Wang, and A. Shreve, "A joint theoretical and experimental study of phenylene-acetylene molecular wires," *Chemical Physics Letters*, vol. 401, pp. 149–156, Jan. 2005.

[80] G. Schull and R. Berndt, "Orientationally ordered (7x7) superstructure of C_{60} on Au(111)," *Physical Review Letters*, vol. 99, no. 22, 2007.

[81] P. Han, B. A. Mantooth, E. C. H. Sykes, Z. J. Donhauser, and P. S. Weiss, "Benzene on Au(111) at 4 K: Monolayer growth and Tip-Induced molecular cascades," *Journal of the American Chemical Society*, vol. 126, no. 34, pp. 10787–10793, 2004.

[82] E. M. Purcell, "Life at low reynolds number," *American Journal of Physics*, vol. 45, pp. 3–11, Jan. 1977.

[83] L. Bartels, G. Meyer, and K. Rieder, "Basic steps of lateral manipulation of single atoms and diatomic clusters with a scanning tunneling microscope tip," *Physical Review Letters*, vol. 79, p. 697, July 1997.

[84] M. J. Weaver, X. Gao, and Y. Zhang, "Scanning tunneling microscopy of carbon molecule (C_{60} and C_{70}) on ordered gold (111) and gold (110): molecular structure and electron transmission," *The Journal of Physical Chemistry*, vol. 96, pp. 510–513, Jan. 1992.

[85] R. J. Wilson, G. Meijer, D. S. Bethune, R. D. Johnson, D. D. Chambliss, M. S. de Vries, H. E. Hunziker, and H. R. Wendt, "Imaging C_{60} clusters on a surface using a scanning tunnelling microscope," *Nature*, vol. 348, no. 6302, pp. 621–622, 1990.

[86] E. Altman and R. Colton, "Nucleation, growth, and structure of fullerene films on Au(111)," *Surface Science*, vol. 279, no. 1-2, pp. 49–67, 1992.

[87] E. I. Altman and R. J. Colton, "The interaction of C_{60} with noble metal surfaces," *Surface Science*, vol. 295, pp. 13–33, Sept. 1993.

[88] E. I. Altman and R. J. Colton, "Determination of the orientation of C_{60} adsorbed on Au(111) and Ag(111)," *Physical Review B*, vol. 48, p. 18244, Dec. 1993.

[89] S. Gangopadhyay, R. A. J. Woolley, R. Danza, M. A. Phillips, K. Schulte, L. Wang, V. R. Dhanak, and P. J. Moriarty, "C60 submonolayers on the Si (111)-(7x7) surface: Does a mixture of physisorbed and chemisorbed states exist?," *Surface Science*, vol. 603, no. 18, p. 28962901, 2009.

[90] J. N. Hohman, P. Zhang, E. I. Morin, P. Han, M. Kim, A. R. Kurland, P. D. McClanahan, V. P. Balema, and P. S. Weiss, "Self-Assembly of carboranethiol isomers on Au(111): Intermolecular interactions determined by molecular dipole orientations," *Nano*, vol. 3, no. 3, p. 527, 2009.

[91] T. Baše, Z. Bastl, M. Šlouf, M. Klementová, J. Šubrt, A. Vetushka, M. Ledinský, A. Fejfar, J. M. cek, M. J. Carr, and M. G. S. Londesborough, "Gold micrometer crystals modified with carboranethiol derivatives," *The Journal of Physical Chemistry C*, vol. 112, no. 37, pp. 14446–14455, 2008.